VOLUME 71, NUMBER 14 JOC Perspective JULY 7, 2006

Energy, Charge, and Spin Transport in Molecules and Self-Assembled Nanostructures Inspired by Photosynthesis

Michael R. Wasielewski

Department of Chemistry and International Institute for Nanotechnology, Northwestern University, Evanston, Illinois 60208-3113

m-wasielewski@northwestern.edu

Received February 2, 2006

Electron transfer in biological molecules provides both insight and inspiration for developing chemical systems having similar functionality. Photosynthesis is an example of an integrated system in which light harvesting, photoinduced charge separation, and catalysis combine to carry out two thermodynamically demanding processes, the oxidation of water and the reduction of carbon dioxide. The development of artificial photosynthetic systems for solar energy conversion requires a fundamental understanding of electron-transfer reactions between organic molecules. Since these reactions most often involve single-electron transfers, the spin dynamics of photogenerated radical ion pairs provide important information on how the rates and efficiencies of these reactions depend on molecular structure. Given this knowledge, the design and synthesis of large integrated structures to carry out artificial photosynthesis is moving forward. An important approach to achieving this goal is the development of small, functional building blocks, having a minimum number of covalent bonds, which also have the appropriate molecular recognition sites to facilitate self-assembly into a complete, functional artificial photosynthetic system.

Introduction

The importance and complexity of electron-transfer reactions in Nature has led many researchers to look for ways to duplicate the fundamental features of these reactions in simplified chemical systems. A vital part of this research is the design and synthesis of molecular systems, comprised of electron donors and acceptors, which mimic photochemical charge separation in photosynthetic proteins. Artificial photosynthetic systems for production of practical solar fuels must collect light energy, separate charge, and transport charge to catalytic sites where water oxidation and CO_2 reduction will occur. While some progress has been made on each aspect of this complex problem, researchers have not yet developed components that are both efficient and robust and have not yet integrated the existing functional components into a working system. The design and development of light-harvesting, photoconversion, and catalytic modules capable of self-ordering and self-assembling into an integrated functional unit will make it possible to realize an efficient artificial photosynthetic system.

Synthetic electron donor−acceptor systems have been prepared to study the dependencies of electron-transfer rate constants on donor−acceptor distance and orientation, free energy of reaction, and electronic coupling. The most informative systems are those in which there are structural constraints to control both the distance and orientation between the electron donors and acceptors. Along with ease of synthesis and stability, bio-inspired systems for photochemical solar energy conversion require components with intense electronic absorptions that cover the solar spectrum. As is the case in photosynthetic reaction center proteins, multicomponent donor−acceptor arrays that carry out multistep charge separation reactions are most useful for producing long-lived charge-separated states.

Many bio-inspired systems employ chromophores with large, conjugated π-systems, such as porphyrins, which are most often synthetically easier to incorporate into complex donor−acceptor systems than are natural chlorophylls and bacteriochlorophylls. Porphyrins are frequently used as both donors and acceptors in these arrays, while aromatic amines and carotenoids serve as secondary electron donors. In addition, fullerenes, quinones, and aromatic imides and bis(imides) are common acceptors because of their low reduction potentials and stable anions. Unambiguous identification of both the short and long-lived radical ions produced by photoinitiated electron transfer is critical to determining the mechanisms by which charge separation and recombination occur in these bio-inspired systems. This information is generally obtained using time-resolved optical and EPR spectroscopy.

10.1021/jo060225d CCC: $33.50
Published on Web 06/30/2006

A key step toward bio-inspired systems for artificial photosynthesis as well as organic electronics in general is the ability to create increasingly larger ordered arrays of interacting molecules. Covalent total synthesis of supramolecular arrays becomes highly inefficient and costly, ultimately requiring the use of self-assembly to achieve ordered complex architectures from properly functionalized building blocks. Despite significant progress in the development of covalent components for artificial photosynthesis, the fundamental concepts of how to prepare individual light-harvesting complexes, reaction centers, or catalysts that can readily engage in specific intermolecular interactions, such as hydrogen bonding, electrostatic, metal−ligand, and $\pi-\pi$ interactions, to self-assemble into ordered supramolecular structures with the ability to function as complete artificial photosynthetic systems, are largely unknown. These structures must provide pathways for migration of light excitation energy among antenna chromophores and from antennas to reaction centers. They must also incorporate charge conduits, i.e., molecular "wires" that can efficiently move electrons and holes between reaction centers and catalytic sites. It is a significant challenge to develop small, functional building blocks, having a minimum number of covalent bonds, which also have the appropriate molecular recognition sites that facilitate self-assembly into complete, *functional* artificial photosynthetic assemblies.

We have recently developed a wide variety of bio-inspired building blocks that can serve to capture light energy, separate charge, and transport charge over long distances. In addition, we have explored how to self-assemble these building blocks into photofunctional structures of interest to artificial photosynthesis. This Perspective will describe several aspects of this work including (1) mapping the relationship between molecular structure and charge separation lifetimes in photogenerated radical ion pairs using spin dynamics; (2) designing molecular wires for long distance charge transport; (3) exploring the nature of through-space electron transfer; (4) developing both covalent and self-assembled molecular dimers capable of excited-state symmetry-breaking leading to charge separation; and (5) self-assembly of light harvesting structures that elicit emergent reaction center function.

Bio-inspiration from Photosynthesis

Photosynthetic organisms are ubiquitous on Earth and, in fact, responsible for the development and sustenance of all life on the planet. Among the different classes of photosynthetic organisms, many types of light-harvesting and electron transport systems are used.[1] However, they all use the same basic strategy, in which light is initially absorbed by antenna proteins containing many chromophores, followed by energy transfer to a specialized reaction center protein, in which the captured energy is converted into chemical energy using electron-transfer reactions.

In green plants, algae and cyanobacteria, photosystem I (PSI)[21] functions to produce NADPH that is used to reduce carbon dioxide in the reactions of the Calvin cycle, while photosystem II (PSII)[44] catalyzes one of the most thermodynamically demanding reactions in biology: the conversion of light energy into redox agents capable of oxidizing water.[2] Photosynthetic bacteria are more primitive, dating from the time when Earth had a reducing atmosphere, and as a consequence have simpler photoconversion pathways. The primary energy and electron-transfer processes in purple non-sulfur bacteria have been studied extensively and have served as the principal inspiration for biomimetic studies over the past 30 years.

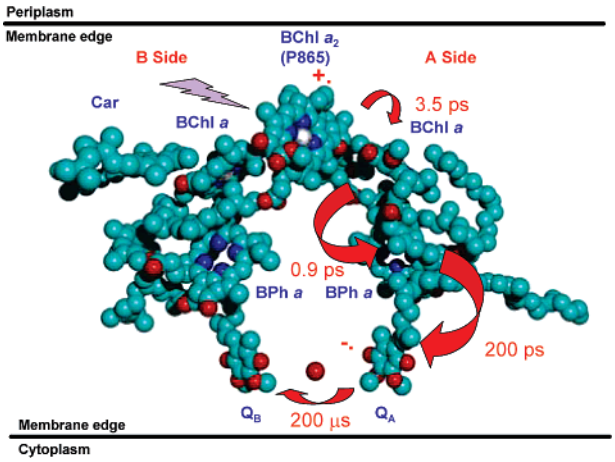

FIGURE 1. Primary charge separation in the photosynthetic RC of purple bacteria. The protein has been removed; only the redox cofactors are shown.

X-ray structures of the purple bacterial reaction center (RC) proteins reveal three subunits, two of which are membrane spanning proteins having an intriguing pseudo 2-fold symmetry.[3−5] These subunits organize the redox cofactors into two parallel arrays, termed the A-side and B-side, leading from the primary electron donor (P865) comprised of a special pair of bacteriochlorophyll molecules, to the quinone electron acceptors (Q_A and Q_B), Figure 1. However, the bacterial RC only utilizes the A-side cofactors for electron transfer. Excitation of P865 produces its lowest excited singlet state that donates an electron to an adjacent bacteriopheophytin (BPh) in ∼3 ps, a process mediated by an accessory BChl interposed between P865 and BPh. This mediation takes place either by direct formation of a $P865^{+\bullet}-BChl^{-\bullet}$ intermediate, or through the virtual participation of this state in a superexchange interaction (see below).[1] The electron then moves to ubiquinone Q_A in ∼200 ps and is subsequently transferred to Q_B in ∼200 μs.[6] When both Q_A and Q_B are either removed or chemically reduced prior to excitation of the RC, formation of $P865^{+\bullet}$-$BPh^{-\bullet}$ is followed by charge recombination in ∼10 ns. This recombination reaction produces a ∼50% yield of ^{3}*P865, whose triplet sublevels are populated in a non-Boltzmann fashion. As a result, the EPR spectrum of this triplet state bears an unusual spin polarization that is the unique signature of charge recombination within a weakly coupled, spin-correlated radical pair.[7,8]

Understanding the nature of electron-transfer reactions as a general phenomenon is essential to developing a clear picture of how photosynthetic charge separation and storage occur. Moreover, this knowledge allows for the development of key design criteria for preparing bio-inspired systems for fuel production through artificial photosynthesis and for the development of organic photovoltaics. These principles will be discussed in the next section.

Design Principles for Bio-Inspired Electron-Transfer Systems

The dependence of the rates of electron-transfer reactions within covalently linked donor−acceptor molecules on the free energy of reaction and the electronic interaction between the

donor and the acceptor are described well by theory developed by Marcus, Levich, Hush, and Jortner.[9−12] Equation 1 shows how the rate depends on these quantities

$$k_{ET} = \frac{2\pi}{\hbar} V_{DA}{}^2 \left(\frac{1}{(4\pi\lambda kT)^{1/2}}\right) e^{-(\Delta G^0+\lambda)^2/4\lambda kT} \quad (1)$$

where $\Delta G°$ is the free energy of reaction, V_{DA} is the electronic coupling between the donor and acceptor, and λ is the total energy of the nuclear reorganization (structural change) within the donor, acceptor, and solvent required for the reaction to occur. One of the key features of eq 1 is that it predicts that the rate of an electron-transfer reaction will slow when the free energy of reaction becomes very large. This is important for maximizing the rate of charge separation, while at the same time minimizing the rate of the energy-wasting charge recombination. Covalent donor−acceptor molecules have been used to establish the existence of the so-called Marcus "inverted region" for charge shift reactions,[13] as well as for charge separation and recombination reactions.[14] The key to observing the inverted region in donor−acceptor molecules is maintaining a fixed distance between the donor and the acceptor as the structure of the donor and/or the acceptor is changed to modify the free energy.

At long distances, the amplitudes of the wave functions of D and A decrease exponentially, and thus, the magnitude of V_{DA}^2 also decreases exponentially as a function of distance. Empirically, the dependence of electron-transfer rate constant on D−A distance in a specific solvent takes on the form given by eq 2

$$k_{ET}(r) = k_0 e^{-\beta(r-r_0)} \quad (2)$$

where r is the donor−acceptor distance, r_0 is the distance, usually van der Waals contact, at which the largest rate occurs, and β is a constant. The largest rate k_0 is usually thought to be close to the frequency of a single molecular vibration, $\sim 10^{13}$ s^{-1}. Experiments have shown that the overall distance dependence of k_{ET} is indeed exponential and is modulated by the geometry of the intervening molecular spacer group provided that the spacer molecule has molecular orbitals that are energetically far removed from those of the donor and acceptor (see below). The exponential dependence of electron transfer rates as a function of distance has been determined using compounds in which the distance between the donor and the acceptor is varied systematically using a rigid hydrocarbon framework.[15] For instance, β values of 1.0−1.4 $Å^{-1}$ for proteins,[16,17] ≤0.2−1.4 $Å^{-1}$ for DNA,[18,19] 0.8−1.0 $Å^{-1}$ for saturated hydrocarbon bridges,[20,21] and 0.2−0.6 $Å^{-1}$ for unsaturated phenylene,[22−25] polyene,[26−29] and polyyne[30−32] bridges have been reported.

Electrons need not transfer from a donor to an acceptor via the direct overlap of their respective orbitals. The spacer or "bridge" molecules that connect the donor and the acceptor may influence the rate of donor−acceptor electron transfer by mixing their electronic states with those of the donor and acceptor. Several virtual states involving the bridge molecule may contribute to the overall electronic configuration of the donor-bridge-acceptor (D−B−A) system. The degree to which each of these virtual states contributes to the overall electronic structure of the system is determined by the magnitude of the electron-exchange interaction involving these states and is generally known as superexchange.[33] Both calculations and experiments have shown that the magnitude of the superexchange contribution to the total donor−acceptor electronic coupling is proportional to donor−acceptor orbital overlap and inversely proportional to the energy gap between the initial donor state and the virtual state involving the bridge molecule.[34] The McConnell model for superexchange[33] predicts an approximately exponential dependence of V_{DA} on the donor−acceptor distance, r_{DA}, an assertion consistently verified by experimental data.[15,35,36] As the length of a bridge increases and the superexchange interaction decreases, electron transfer can only occur by direct oxidation or reduction of the bridge molecule, resulting in a sequential electron transfer mechanism involving observable intermediates. Depending on the energies of charge separated states involving the bridge molecules, sequential, wire-like charge transfer, which is also known as "hopping", generally becomes more efficient than superexchange at long distances.[37,38]

The importance of using a cascade of thermal electron-transfer steps following the initial photoinduced charge separation to increase charge separation lifetimes, as evidenced by natural photosynthesis, has been demonstrated in numerous systems (reviewed in refs 39−44). Studies on the optimization of the free energy changes, distances, and orientations between the various donors and acceptors have determined strategies for the development of novel molecular structures to tailor the charge separation and storage characteristics to specific applications. For example, efficient performance in the solid state requires the use of specialized donor and/or acceptor molecules that minimize the reorganization energy λ, such as a C_{60} electron acceptor, and/or the incorporation of high potential donors and acceptors to overcome the inability of the solvent to reorganize in the solid state.[45] The effect of λ is illustrated in the case of **1**, where excitation of the porphyrin in this carotenoid (C) porphyrin (P) quinone (Q) molecular triad yields the porphyrin first excited singlet state, $C-{}^1*P-Q$, which decays via a sequential, two-step, electron-transfer process into a $C^{+\bullet}-P-Q^{-\bullet}$ charge-separated state with a lifetime of 0.17−2.5 μs and quantum yields >25% depending on solvent.[46] When C_{60} is substituted for the quinone as the acceptor, the quantum yield of $C^{+\bullet}-P-C_{60}{}^{-\bullet}$ is relatively constant under conditions ranging from fluid solution at ambient temperatures to a rigid glass at 8 K reaching up to 0.88 with a microsecond lifetime, depending upon the conditions.[47] Redox cascades having as many as four steps have been demonstrated.[48]

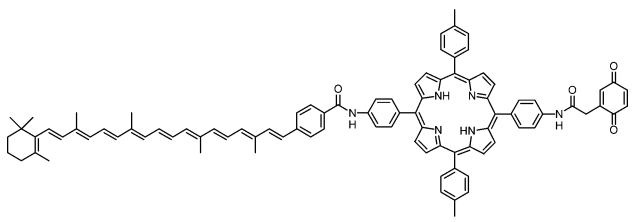

1

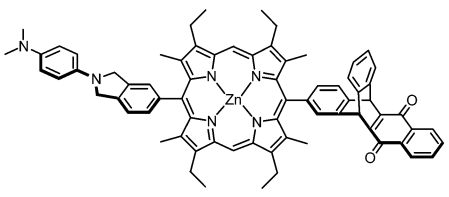

2

We have developed reaction free energy criteria for achieving high quantum yield charge separation in donor−acceptor systems in the solid state at cryogenic temperatures.[45] Briefly, when the motion of a polar solvent is restricted, as occurs when it is cooled to a glassy state, its dielectric constant decreases to that of a nonpolar solvent. Under these conditions, the solvent stabilizes a photogenerated ion pair very little, so that the energy of the ion pair is about 0.75 eV higher in the glassy solvent than it is in the corresponding polar liquid. Using this information as a predictive model, we prepared molecule **2**, which consists of a zinc porphyrin (ZP) primary electron donor positioned between a naphthoquinone (NQ) electron acceptor and a phenylenediamine (PD) secondary electron donor.[49] Molecule **2** demonstrates two-step, sequential charge separation at 5 K to yield a radical ion pair (RP) that possesses an overall 23-Å center-to-center distance, a 4-ms lifetime, and exhibits the spin polarization characteristic of $P865^{+\bullet}-Q_A^{-\bullet}$ in photosynthetic RCs as indicated by EPR spectroscopy. However, charge recombination leads directly to ground state because the energy of ^{3}*ZP is above that of the radical pair.

The most difficult properties of the photosynthetic RC to model simultaneously are the strong electronic coupling leading to ultrafast charge separation and the subsequent weak coupling producing the observed spin dynamics, all in a system in which the electron donors and acceptors have highly restricted distances and orientations between them. This contrasts sharply with noncovalent radical pair chemistry observed in solution, where rapid radical pair formation followed by diffusive radical separation to long distances and subsequent re-encounter results in chemically induced electron and nuclear polarization (CIDEP and CIDNP) phenomena.[50] Modeling all aspects of the RC protein spin dynamics is important because they directly reflect the dependence of V_{DA}^2 on molecular structure, which is discussed in detail in the next section. An important part of this modeling is to understand how RP recombination leads to triplet states with unusual spin polarization as is observed in photosynthetic RCs and, thus, how synthetic structures that target photochemical energy conversion can be optimized to slow energy-wasting charge recombination.

The observation of a spin-polarized RP following photoexcitation of the PD−ZP−NQ triad, **2**, prompted us to develop a more complex system in an attempt to obtain the correct energetics that would result in back reaction to a spin polarized triplet state as is observed in photosynthetic RCs. We chose to replace the PD donor with a chlorophyll derivative that possesses a triplet state at 1.4 eV and is about 0.2 V harder to oxidize than PD, so that the energetics for charge recombination to the chlorophyll triplet are favorable.[51] Photoexcitation of chlorophyll−porphyrin−quinone triad **3** once again resulted in formation of a long-lived, spin-polarized RP, yielding an 8-ms RP lifetime at 5 K, but unfortunately did not show a significant rate of charge recombination leading to the chlorophyll triplet state. Given the lengthy synthetic pathway necessary to prepare **3**, we decided to investigate simpler structures that could be modified more easily to probe the structural issues that most likely were behind the inability of the earlier models to completely mimic all the spin dynamics of the photosynthetic RC.

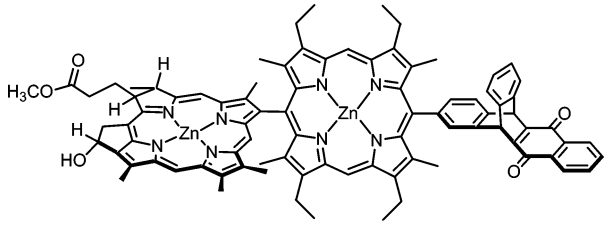

3

The Link between Spin Dynamics and Electron-Transfer Mechanisms

As mentioned above, superexchange is thought to be an important mechanism for efficient electron transfer within the photosynthetic RC[52,53] and has been studied in various biomimetic systems.[54,55] The term was first used by Kramers[56] and later by Anderson[57,58] to describe the indirect exchange coupling of unpaired spins via filled orbitals which acquire paramagnetic character through mixing with charge-transfer excited-state configurations.[58] The rates of nonadiabatic electron-transfer reactions, k_{ET}, depend directly on V_{DA}, eq 1, whose magnitude gives the effective interaction energy between the relevant orbitals on the donor and acceptor.[12,59] When the electron-transfer reaction originates from a state in which the redox centers are also paramagnetic, e.g., charge recombination from a RP, the superexchange coupling that dictates the electron transfer rates from the RP to energetically proximate electronic states is the same coupling that determines the magnetic interaction between the unpaired spins of the RP.[56−58,60−62] *Therefore, the magnitude of the magnetic interaction between the radicals of the RP and its behavior mirrors that of* V_{DA}.

Experimentally, the magnetic field effect (MFE) on the yield and rate of RP recombination can directly reveal the magnitude of the electron spin−spin exchange interaction, 2*J*, between the spins within the RP, which is proportional to V_{DA}^2.[63−66] The mechanistic details of the radical pair intersystem crossing mechanism (RP−ISC) and the theory behind the MFE have been researched extensively[67−70] and applied to many donor−acceptor systems[25,71−78] including biological systems.[68,79−82] Following charge separation, the RP, initially formed in its singlet configuration, undergoes electron−nuclear hyperfine coupling-induced RP-ISC to produce the triplet RP, Figure 2A. The subsequent charge recombination process is spin selective; i.e., the singlet RP recombines to the singlet ground state and the triplet RP recombines to yield the neutral local triplet. Application of a magnetic field results in Zeeman splitting of the RP triplet sublevels, which at high fields can be described by the T_0 and $T_{\pm1}$ states, Figure 2B. In the high-field limit, population of the RP triplet state occurs exclusively by $S-T_0$ mixing, while T_{-1} and T_{+1} remain unpopulated. If $2J < 0$, the singlet energy level is below that of the triplet sublevels, Figure 2B, so that when the Zeeman energy from the applied field equals that of the S−T splitting, T_{-1} crosses the singlet and the RP-ISC rate is maximized, which should produce a resonance in the triplet yield at B_{2J}, directly yielding 2*J*.[58,83] If $2J > 0$, the singlet energy level is above that of the triplet sublevels, and S crosses T_{+1} yielding the same information. The appearance of a distinct resonance depends critically on having a RP in which the two radicals have a relatively narrow distribution of distances and orientations between them. As a consequence, the observed resonances are exquisitely sensitive to molecular structure. An increase in the rate of triplet formation at resonance implies

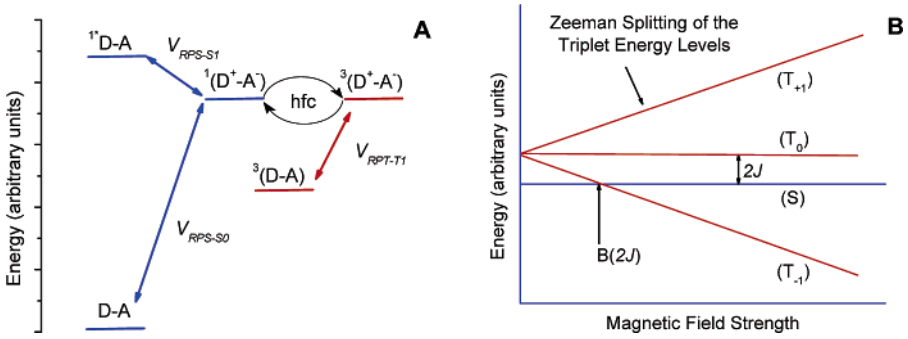

FIGURE 2. (A) Energy level diagram. (B) Radical ion pair energy levels as a function of magnetic field.

that the RP decay rate also increases. One can therefore monitor the RP population as a function of applied magnetic field and obtain a plot with a minimum at B_{2J} to obtain $2J$ as well.

Optically detected MFE measurements on reactant or product yields do not, however, show how the spin polarization of the radicals within the RP evolves with time, how the structure of radicals may be changing, or how the dynamics of the medium couple with the spin dynamics of the radical pairs. Time-resolved electron paramagnetic resonance spectroscopy (TREPR) yields this information directly.[84] At the 350 mT magnetic field typical of EPR experiments at X-band, when the $D^{+\bullet}-B-A^{-\bullet}$ RP distances are 15−20 Å, $2J$ is generally about 0.1−1 mT, so that preferential $S-T_0$ mixing occurs within $D^{+\bullet}-B-A^{-\bullet}$.[75,76,85−88] The resultant spin-correlated radical pair states can be identified through the unique polarization of the EPR transitions that occur between these states.[89,90] If $2J$ is larger, as may be the case when the $D^{+\bullet}-B-A^{-\bullet}$ distance is small, mixing of the S state of the radical pair with either T_{-1} ($2J < 0$) or T_{+1} ($2J > 0$) may also occur, which results in different polarization of the EPR transitions relative to those that result from $S-T_0$ mixing. The non-Boltzmann spin populations within the radical ion pair are transferred to the neutral triplet state ^{3}*(D−B−A) that results from radical ion pair recombination within $^3(D^{+\bullet}-B-A^{-\bullet})$.[91,92] The polarization of the EPR transitions exhibited by a triplet formed by the ordinary spin−orbit intersystem crossing (SO-ISC) mechanism can be differentiated from the RP-ISC mechanism by the polarization pattern of the six EPR transitions at the canonical orientations.[92] In SO-ISC, the three zero-field levels are selectively populated, and this selectivity is carried over to the high-field energy levels. RP-ISC acts directly on the high-field triplet sublevels via singlet−triplet mixing $S-T_0$ (or $S-T_{\pm1}$). Thus, SO-ISC results in mixed absorption (a) and emission (e) lines for the two EPR transitions $T_i \leftrightarrow T_o$ (where $i = \pm1$) associated with each orientation (x, y, z), while in RP-ISC a mixed polarization pattern is impossible. For example, the (a,e,e,a,a,e) polarization pattern of the six EPR transitions from low to high field can only be attributed to the RP-ISC mechanism.

Rodlike Electron Donor−Acceptor Systems That Mimic Reaction Center Function

In developing a simplified approach to mimicry of RC function, we decided to investigate chromophores having a lowest excited singlet state with significant charge transfer character that could promote directional charge separation. Combining these chromophores with donors and acceptors into multistep electron-transfer systems using a small number of synthetic steps allowed for the investigation of a large number of related structures. We initially selected 4-(*N*-piperidinyl)-aminonaphthalene-1,8-dicarboximide (6ANI) derivatives to accomplish this goal. We prepared a simple donor−acceptor triad, **4**, in four steps starting from commercially available compounds.[93] The *p*-methoxyaniline (MeOAn) serves as an electron

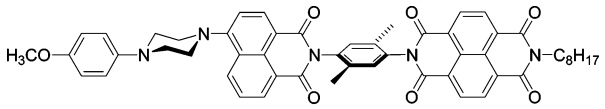

4

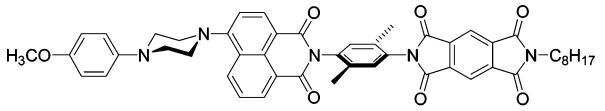

5

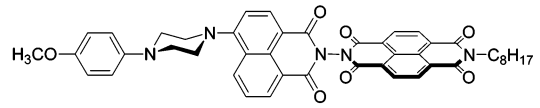

6

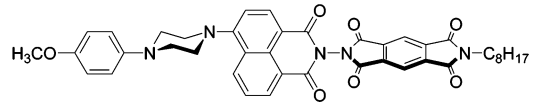

7

donor, while the naphthalene-1,8:4,5-bis(dicarboximide) (NI) is an electron acceptor. This rodlike system has excellent spatial control of the distance and orientation of the donors and acceptors. Photoexcitation of the 6ANI chromophore at 400 nm results in formation of a CT singlet state, ^{1}*6ANI, followed by two sequential nonadiabatic electron-transfer reactions, Figure 3A, where $k_{CS1} = 1.3 \times 10^{11}$ s^{-1} and $k_{CS2} = 2.3 \times 10^9$ s^{-1}.[93] The rapid charge separation photochemistry mimics that of the photosynthetic RC and results in formation of a spin-correlated radical pair in which the spins are initially in the singlet configuration (RP_S). RP-ISC induced largely by electron−nuclear hyperfine interactions results in formation the triplet radical pair (RP_T). Spin-selective charge recombination results in repopulation of the ground state as well as formation of the neutral triplet state localized on NI. The NI triplet state exhibits the spin-polarized EPR spectrum (a,e,e,a,a,e) characteristic of the spin-correlated radical pair precursor, Figure 3B. As a result, this very simple chemical system gave us the first entry point into modeling the subtleties of how molecular structure affects electronic coupling in the RC.

In these first TREPR experiments on **4**, liquid crystal (LC) solvents were used to aid in the elucidation of the electron-

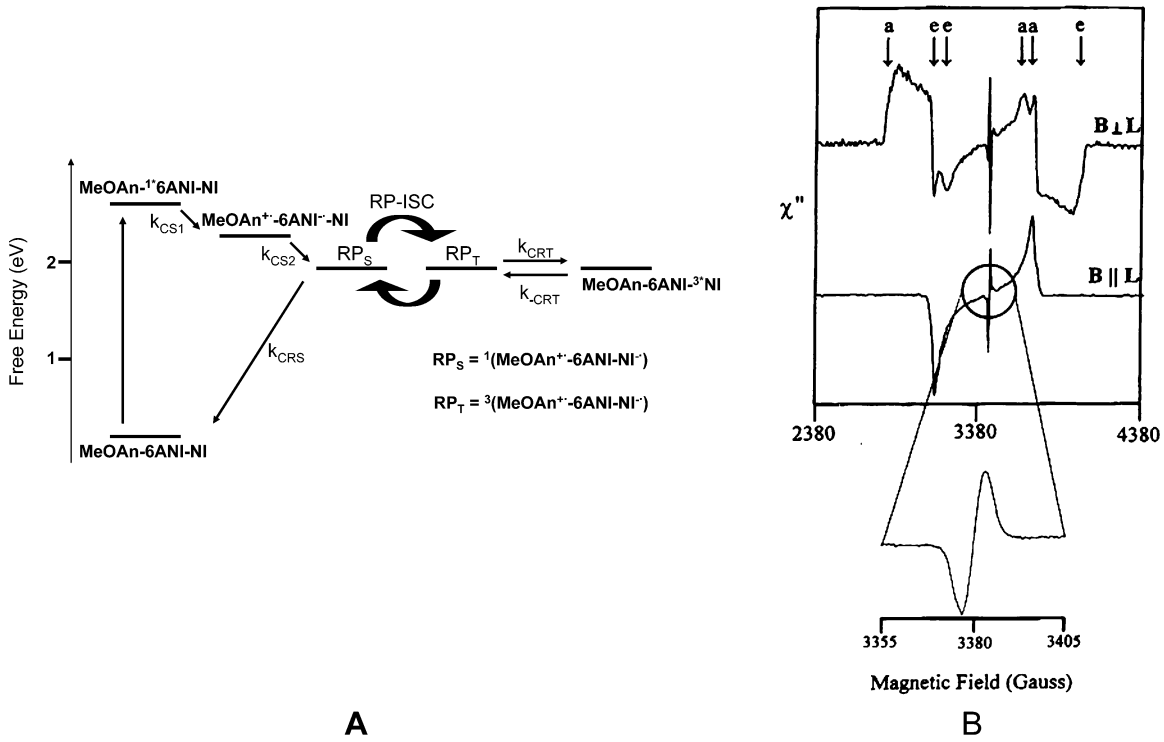

FIGURE 3. (A) Light-driven electron-transfer pathway for **4**. (B) TREPR of **4** in the nematic LC mixture Merck E-7 at 100 K. The spectra are shown with the direction of the magnetic field, **B**, parallel and perpendicular to the LC director, **L**. The inset shows the RP signal.

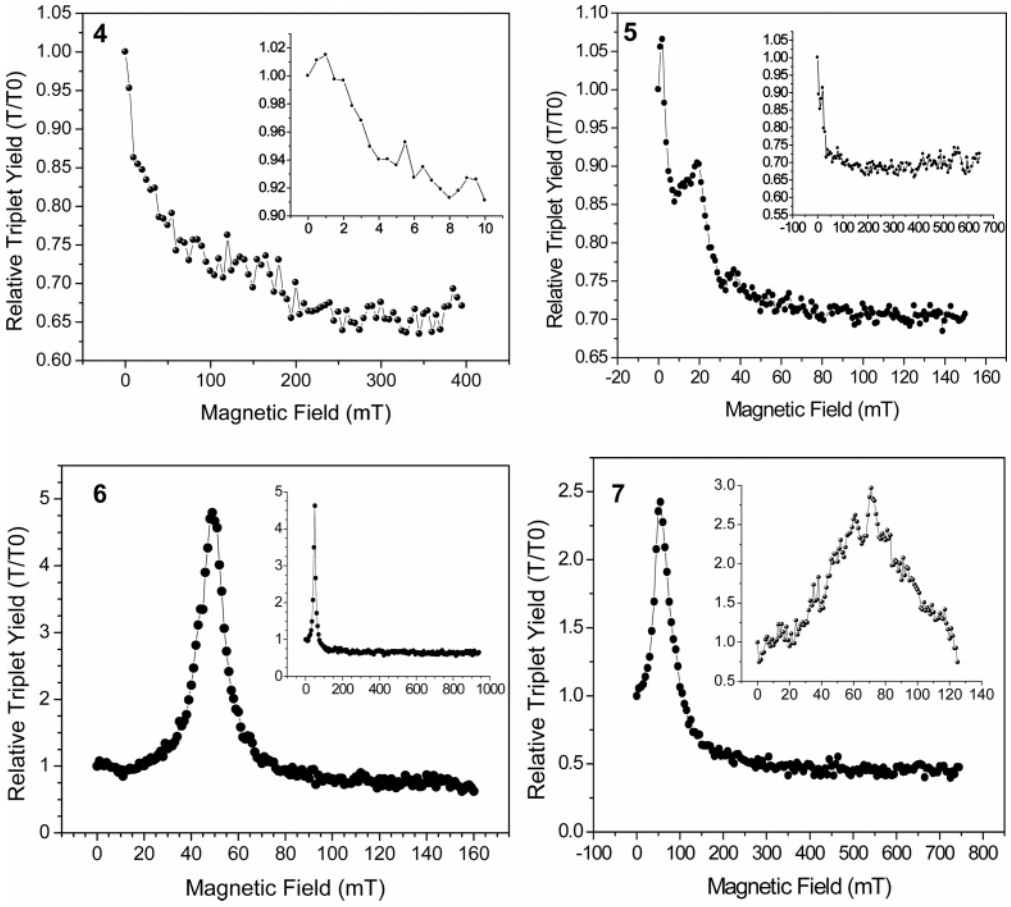

FIGURE 4. Triplet yields as a function of magnetic field for **4**−**7**. The insets provide expanded or contracted views of the data.

transfer mechanism and the spin dynamics.[93,94] The solvation properties of LCs make them very useful for this purpose because of (1) their ability to partially orient the donor−acceptor molecules, making it possible to study the effects of anisotropic

media on the electron-transfer process, (2) their unique dielectric properties that serve to slow electron-transfer rates, and (3) the wide temperature range over which TREPR spectra of RPs and triplet states can be observed in LCs.

Mapping the Dependence of Electronic Coupling on Structure Using Spin Dynamics

We have measured 2*J* using magnetic field effects on the triplet yields resulting from RP-ISC followed by charge recombination in triads **4**−**7**.[75] Two-step charge separation from the lowest excited singlet state of 6ANI yields singlet radical ion pairs in which the charges are separated by 14−19 Å and whose lifetimes range from about 15 to 200 ns. These lifetimes are long enough so that RP-ISC occurs to form the triplet radical ion pair, which then recombines to form a neutral excited triplet state localized on NI in **4** and **6** and on 6ANI in **5** and **7**. The yield of this locally excited triplet state, monitored by nanosecond transient absorption as a function of applied magnetic field strength, exhibits distinct resonances that directly yield 2*J*, Figure 4. These measurements provide a highly sensitive method for determining the dependence of the electronic coupling for charge recombination on the structure of the radical ion pair, which is essential for optimizing systems for photochemical conversion and storage of solar energy. For example, molecules **6** and **7**, which lack the phenyl spacer group, show values of 2*J* that are about 30 times larger than those of **4** and **5** in which the phenyl is present. In addition, the two distinct resonances observed for **5** suggest that there are two slightly different conformations that result in two different values of V_{DA} at room temperature. Electron transfer rates depend directly on V_{DA}, which is very sensitive to the conformation of the D−B−A molecule as well as the distance between the donor and the acceptor. As a result, conformational dynamics can exert considerable control over electron-transfer reactions. These dynamics can be studied by taking advantage of the relationship of 2*J* to V_{DA}^2. Our recent detailed studies of **6** illustrate this point.

Photoinitiated two-step charge separation with **6** produces ^{1}(MeOAn$^{+\bullet}$−6ANI−NI$^{-\bullet}$). RP-ISC subsequently produces ^{3}(MeOAn$^{+\bullet}$−6ANI−NI$^{-\bullet}$), and the total RP population decays with a ∼10 ns lifetime at 140 K in toluene, which increases to nearly 30 ns at 300 K. The activation energy observed for this process is *negative* and can be explained by a mechanism involving a conformational preequilibrium of the RP followed by charge recombination. Over the same temperature range, the MFE on the yield of the triplet recombination product, MeOAn−6ANI−^{3}*NI, yields the magnitude of 2*J*, which directly monitors the superexchange electronic coupling for charge recombination. A single resonance in the MFE plot is observed at 300 K, which splits into two resonances at temperatures below 230 K, suggesting that there are two distinct groups of RP conformations at low temperature, Figure 5. The magnitude of 2*J* for the lower field resonance (10 mT) at 140 K is five times smaller than that of the high-field resonance. At 300 K, the equilibrium is shifted almost entirely to the set of conformers with the stronger electronic coupling. The motion that couples these two groups of conformations is the motion that most effectively gates the donor−acceptor electronic coupling. There is evidence to suggest that electron transfer within this molecule may be significantly influenced by molecular motions within 6ANI.[95−97]

We have expanded the use of MFE measurements to probe superexchange-mediated through-space electron-transfer mechanisms using u-shaped molecules **8**−**11**.[98] The mechanistic possibilities tested by these molecules are summarized in Figure 6, where a rigid intramolecular Donor−Acceptor(1)−Bridge−Acceptor(2)−X system is folded into a u-shape, in which the X group can engage in a nonbonded interaction with the primary electron acceptor or donor during charge separation and/or recombination. In addition, solvent molecules that are positioned in the groove between the donor and acceptor may provide

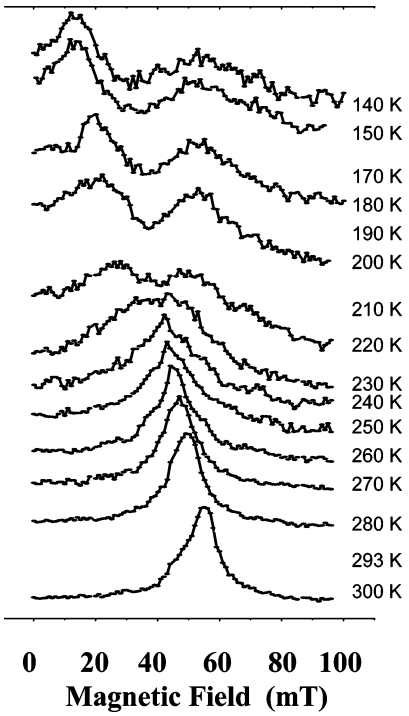

FIGURE 5. Triplet yield vs magnetic field plots for **6**, MeOAn-6ANI-NI, as a function of temperature normalized in amplitude so that positions of the *2J* resonances along the magnetic field axis are highlighted.

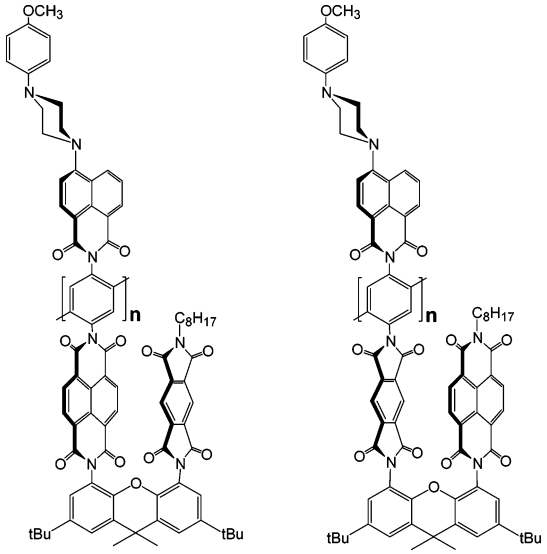

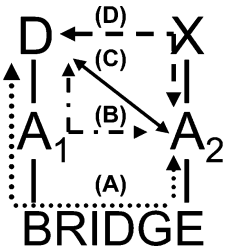

FIGURE 6. ET pathways.

another pathway for electron transfer. Apart from the trivial case of a sequential electron-transfer mechanism involving real intermediates, charge separation and recombination between D and A_2 can occur by four main pathways, Figure 6. The through-bond pathway A between D and A_2 for molecules **8**−**11** is by design much too long to allow rapid charge separation or recombination to occur. In pathway B, a through-bond interaction between D and A_1 is followed by a direct through-space interaction between A_1 and A_2. In pathway C, electron transfer may occur by direct through-space orbital overlap of D and A_2. Last, in pathway D, electron transfer can occur by means of a superexchange interaction involving the orbitals of substituents X of A_2 that are close to D, yet are not directly bonded to it. In addition, superexchange involving solvent molecules positioned between D and A_2 may also be considered as a variant of this pathway. In most molecules, several of these electron-transfer pathways operate simultaneously, and the challenge is to factor the contributions of each pathway to the overall electron-transfer rate.

Femtosecond and nanosecond transient absorption spectroscopy was used to explore the relative efficiency of through-bond and through-space electron transfer in these molecules. The magnitude of the electronic coupling between the oxidized donor and the reduced acceptor was probed specifically by direct measurements of the singlet−triplet splitting, 2*J*, within the radical ion pairs using MFEs on the yield of triplet states resulting from radical ion pair recombination. These data were used to quantitatively assess the effects of both energetics and electronic coupling on the electron transfer mechanism. Through-space electron transfer was found to be a viable mechanism in the u-shaped structures, when reduction of the acceptor that is folded back toward the donor is energetically more favorable than reduction of the acceptor directly bonded to the donor.

Achieving Wire-like Charge Transport

The effectiveness of long-distance charge transport in molecules is dictated by whether strongly distance-dependent superexchange or weakly distance-dependent charge hopping mechanisms dominate. Optimizing molecular structures to accentuate the latter process is the key to producing wire-like behavior in molecules for use in photochemical energy conversion. To achieve this goal, one must (1) identify the relative contributions of each mechanism to charge separation, (2) find the link between these contributions and the energy levels of the system, and (3) choose donors, bridges, and acceptors that drive the system toward the hopping mechanism at long distances. We have produced a D−B−A system that addresses these issues directly.[25] It uses a series of *p*-phenylene (Ph_n) oligomers, **12**, where $n = 1-5$, to link a phenothiazine (PTZ) electron donor to a perylene-3,4:9,10-bis(dicarboximide) (PDI) electron acceptor. Selective photoexcitation of PDI within PTZ−Ph_n−PDI results in charge separation to produce a spin-coherent singlet RP, ^{1}(PTZ$^{+\bullet}$−Ph_n−PDI$^{-\bullet}$), which subsequently undergoes RP−ISC to yield ^{3}(PTZ$^{+\bullet}$−Ph_n−PDI$^{-\bullet}$). The triplet RP then recombines to give almost exclusively ^{3}*PDI. The yield of ^{3}*PDI formed via RP−ISC exhibits distinct resonances as a function of applied magnetic field that directly yield 2*J*, Figure 7.

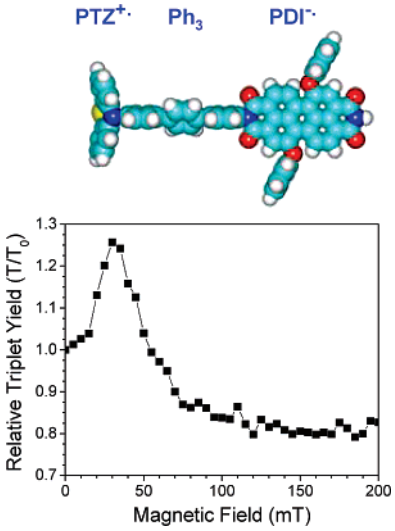

FIGURE 7. Plot of the relative yield of ^{3}*PDI vs magnetic field strength for PTZ-Ph_3-PDI ($2J = 31$ mT).

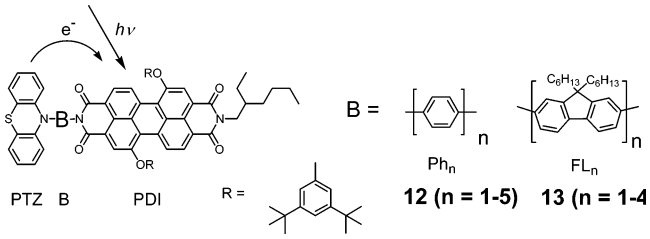

The exponentially decaying rate of charge and spin transfer via superexchange in PTZ$^{+\bullet}$−Ph_n−PDI$^{-\bullet}$ is monitored as the bridge length *n* is increased by directly measuring the distance dependence of 2*J* within the RP, Figure 8A. At the same time, the measured charge recombination rates are nearly distance independent at long distances ($n = 3-5$) showing that charge transport is dominated by hopping, i.e., wire-like behavior, Figure 8B. Thus, the charge recombination mechanism changes dramatically from superexchange to hopping as the bridge is lengthened. Our data support a model in which charge injection from the donor into the bridge leading to wire-like charge transport requires a near-resonant interaction between the state in which the donor is oxidized and that in which the bridge is oxidized. Our results allowed us to dissect for the first time the relative contributions of the superexchange and hopping mechanisms to the overall charge transport process in a conjugated bridge molecule.

In this same series, we recently observed well-defined regions of superexchange and thermally activated hopping in the temperature dependence of charge recombination.[99] Fits to the thermally activated charge recombination rates of **12** ($n = 3$) and ($n = 4$) yield activation barriers of 1290 cm^{-1} and 2030 cm^{-1}, respectively, which match closely the theoretically predicted and experimentally observed barriers for the plan-

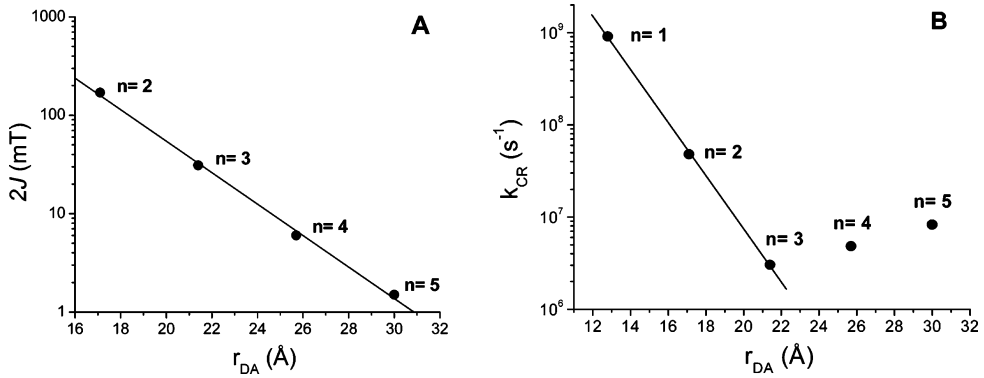

FIGURE 8. Logarithmic plots for **12** of (A) 2*J* vs donor−acceptor distance, r_{DA}, and (B) charge separation rate constant, k_{CS} vs r_{DA}.

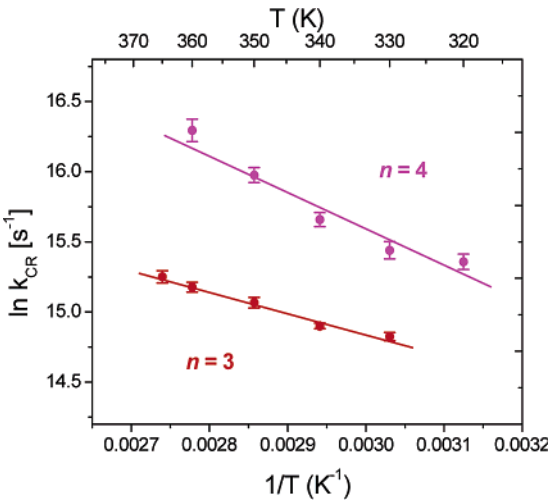

FIGURE 9. Plot of ln k_{CR} vs $1/T$ in the positively activated temperature regions for **12** (n = 3, 4).

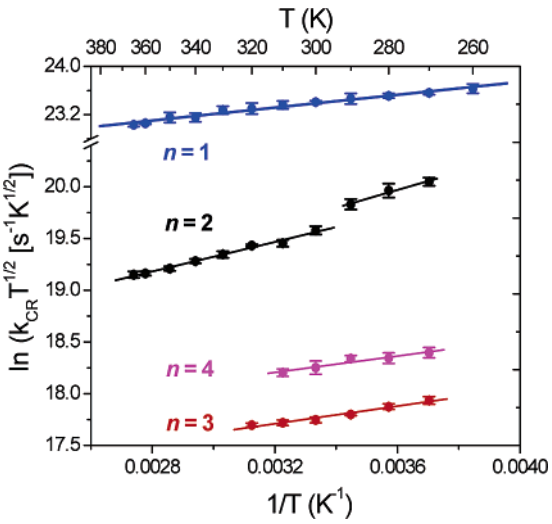

FIGURE 10. Plot of ln($k_{CR}T^{1/2}$) vs $1/T$ in the negatively activated temperature regions for **12** (n = 1−4).

arization of terphenyl and quaterphenyl, respectively, Figure 9.[100,101] Negative activation of charge recombination in the temperature regions dominated by superexchange charge transport is the result of a fast conformational preequilibrium that increasingly depopulates the reactive state for charge recombination as temperature is increased, Figure 10. The temperature dependence of the effective donor−acceptor superexchange coupling, V_{DA}, measured using magnetic field effects on the efficiency of the charge recombination process, shows that charge recombination occurs out of the conformation with lower V_{DA} via the energetically favored triplet pathway. These data strongly indicate that changes in the bridge conformations, which translate into changes in bridge energetics, result in conformational gating of the charge recombination process. This implies that control of bridge conformations may be useful in preventing energy-wasting charge recombination processes. Precise structural control is the hallmark of photosynthetic charge separation.

While the use of rigidly bound D−B−A molecules has simplified the investigation of the distance dependence of electron transfer by keeping the donor−acceptor distance (r_{DA}) well defined, it is difficult to vary r_{DA} by changing the length of the bridge, without substantially altering the energy levels of the bridge. Using a series of D−B−A molecules having PTZ donors, 2,7-oligofluorene (FL_n) bridges, and PDI acceptors, **13**, we have reported the first instance where the distance over which the electron is transferred can be varied *without significantly changing the energies of the relevant bridge states*.[102] Photoexcitation of PDI to its lowest excited singlet state results in oxidation of PTZ via the FL_n bridge. In toluene, the rate constants for charge recombination, Figure 11A, as well as the energy levels of the relevant PTZ−$FL_n^{+\bullet}$−$PDI^{-\bullet}$ bridge states for n = 1−4 are only weakly distance dependent, where the transition between the superexchange and hopping mechanisms occurs at n = 2. Measurements of 2*J*, Figure 11B, and therefore the superexchange interaction, diminish exponentially with distance, Figure 11C, while the overall charge recombination rates through FL_n for n = 3, 4 are dominated by charge hopping. It is clear from these studies that both bridge energetics and molecular motions within D−B−A molecules are very important for accessing efficient mechanisms of charge transport over long distances.

Self-Assembly Strategies for Integrated Photofunctional Nanostructures

Achieving a functional integrated artificial photosynthetic system requires hierarchical organization at both the molecular and supramolecular level. Covalent synthesis provides functional building blocks with well-defined molecular geometries and donor−acceptor distances, while self-assembly provides a facile way to assemble large numbers of molecules into structures that

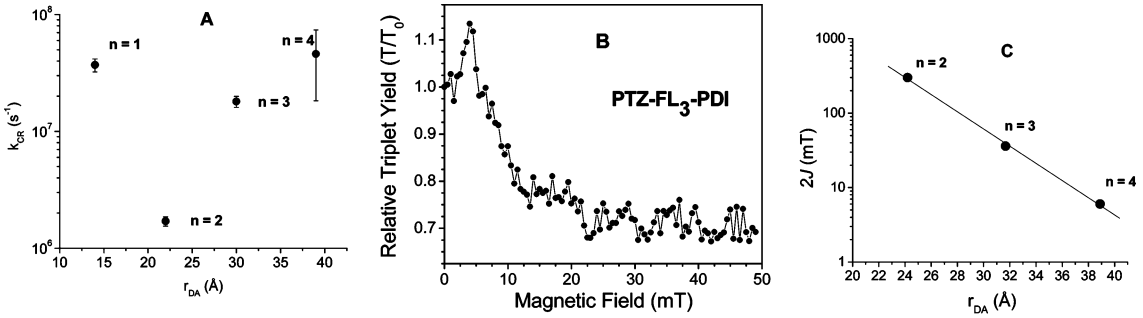

FIGURE 11. (A) Plot of charge recombination vs distance for **13**, $PTZ^{+\bullet}-FL_n-PDI^{-\bullet}$. (B) Plot of relative yield of $PTZ-FL_3-{}^3*PDI$ vs magnetic field. (C) Plot of ln(2*J*) vs distance for $PTZ^{+\bullet}-FL_n-PDI^{-\bullet}$.

can bridge length scales from nanometers to macroscopic dimensions. It can also lead to synergistic and *emergent* properties that are not intrinsic to the building blocks themselves. Our strategy uses covalent building blocks with particular shapes, sizes, and intermolecular interactions, such as $\pi-\pi$ interactions and hydrogen bonding, to direct the formation of supramolecular structures having enhanced energy capture and charge transport properties. We have used time-resolved optical and magnetic resonance techniques to investigate how charge transport depends on supramolecular structure within these systems.

Self-Assembled Light Harvesting Antennae. An antenna, or light-harvesting molecule, is one which increases the cross-section for absorption of solar energy without undergoing charge separation itself. Following photoexcitation, a series of one or more energy-transfer steps occurs, which funnels the excitation energy to a site at which charge separation occurs. In photosynthetic organisms, the use of antenna proteins serves to limit the need for the organism to produce large amounts of the complex charge separation apparatus, while maintaining a high efficiency for light collection by regulating their response to varying light intensity.[103] Covalent light-harvesting chromophoric arrays designed to funnel energy to a central site have been demonstrated.[104−106] These molecules require significant effort to synthesize, such as **14**, where selective photoexcitation of the Zn porphyrins results in rapid energy transfer in about 24 ps to the central metal-free porphyrin.[104] While elaborate and elegant synthetic strategies have led to large arrays of chromophores that can directly transport energy, the ability to create self-assembling antenna arrays that are robust, yet functional, is only beginning. The self-assembly of chlorophyll derivatives similar to those found in green sulfur bacteria into large antenna structures has been explored,[107,108] and new self-assembling antenna systems produced from PDI arrays, such as $(PDI_5)_2$ assembly **15**,[109] take advantage of the robust nature of this dye as evidenced by its use as an industrial pigment.[109]

As an example of the building block approach to a self-assembling antenna structure we have prepared and studied covalent zinc phthalocyanine PDI derivative, **16** ($ZnPcIm_4-PDI_4$). Face-to-face aggregation of **16** is evidenced by its electronic absorption spectra, Figure 12. The spectra show that the aggregated molecule absorbs strongly from 300 to 700 nm, making it an ideal system to harvest polychromatic light. The absorption spectra in both THF and $CHCl_3$ show two broad bands near 500 and 645 nm due to PDI and $ZnPcIm_4$, respectively, which are both strongly blue-shifted relative to the corresponding 548 and 700 nm bands of the monomers.

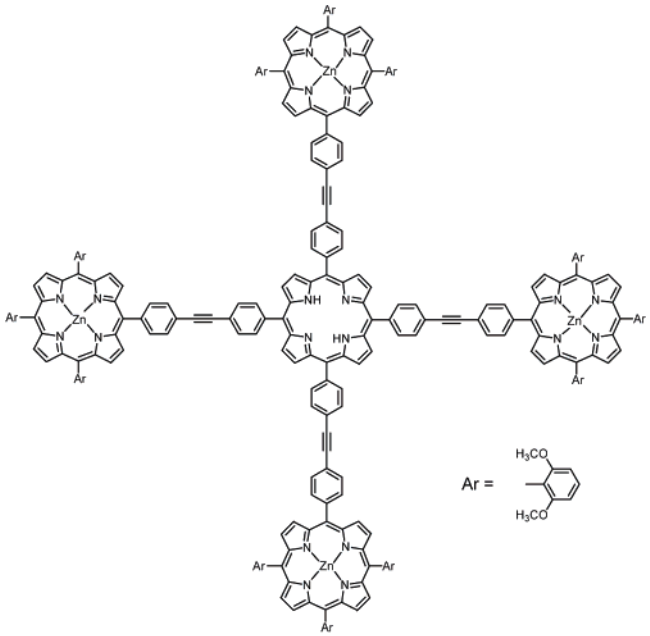

14

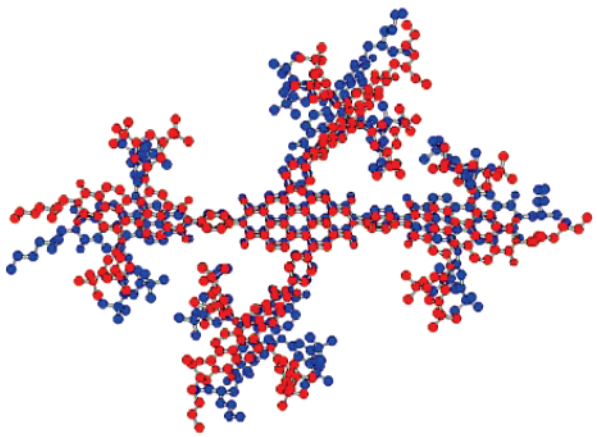

15

Positioning the transition dipoles of two identical chromophores in a parallel, stacked geometry results in exciton coupling of the two transition dipoles causing the lowest energy electronic transition of the dimer to split into two bands, with the higher energy band having enhanced oscillator strength.[110] Our previous studies[109,111] have revealed that PDI readily forms H-aggregates. The broad band near 645 nm is also

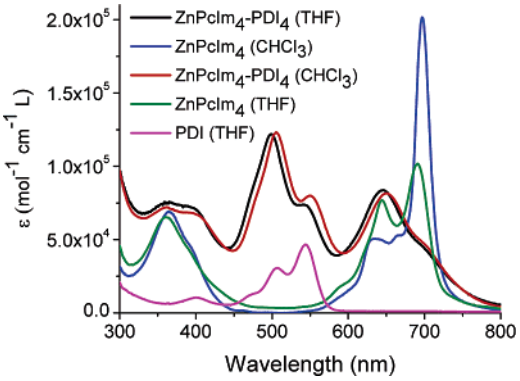

FIGURE 12. UV−vis absorption spectra of **16** and its component chromophores.

characteristic of zinc phthalocyanine H-aggregates.[112] Thus, the electronic absorption spectra strongly support a stacked structure.

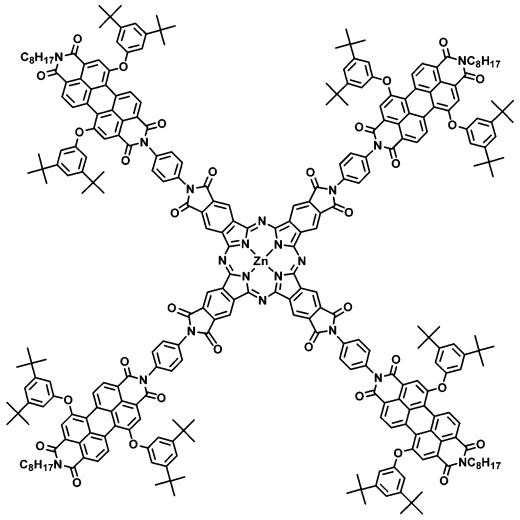

16

To estimate the $ZnPcIm_4-PDI_4$ aggregate structure in solution we performed small-angle X-ray scattering (SAXS) measurements on **16** in THF (6×10^{-4} M) using a high-flux synchrotron source. This is an important new application of a technique that is well-known in the protein structure community, but has only recently been exploited for determining the structures of large molecules and supramolecular assemblies.[113] We believe that this technique is poised to make a major impact on determining supramolecular structures in solution for *concentrations at which direct comparisons can be made with spectroscopic results*. Scattering data obtained in solution is dominated by the solvent, so exceptional signal-to-noise is required to eliminate solvent scattering from that of the solute. So-called third-generation synchrotron X-ray sources, such as the Advanced Photon Source at Argonne National Laboratory, have sufficient brightness to make it possible to obtain the required signal-to-noise ratio with short data collection times. Guinier analysis,[114] reveals that **16** forms monodisperse aggregates in THF (linear Guinier plot) with a radius of gyration $R_g = 21.1$ Å. The monodisperse character of the aggregates of **16** in THF allows an analysis of the scattering data using pair distance distribution function (PDF) and simulated annealing procedures.[115] These methodologies show that the SAXS data is best fit to a stack of seven cofacial

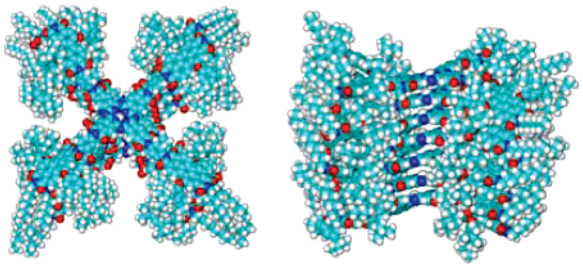

FIGURE 13. Best fit structure of $(\mathbf{16})_7$ aggregates from modeling the SAXS data: left, top view; right, side view.

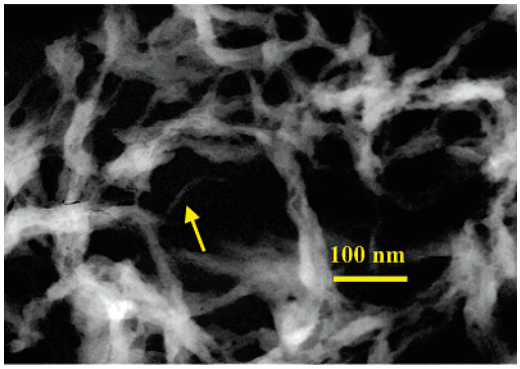

FIGURE 14. TEM image of extended aggregates of **16**.

molecules of **16** with overall dimensions of $6 \times 6 \times 3$ nm, Figure 13.

As the concentration of **16** is increased, the cylindrical stacks grow to form long fibers. The TEM image, Figure 14, of $ZnPcIm_4-PDI_4$ shows fibers longer than 1 μm with different diameters. The smallest discernible fiber diameter in the image is about 5 nm, as indicated by the arrow, which is about the width of a single $ZnPcIm_4-PDI_4$ molecule. These fibers also form ropes, some of which have helical twists, as can be seen just right of center in the image.

Selective photoexcitation of PDI within $(\mathbf{16})_7$ results in formation of ^{1}*PDI, which undergoes singlet−singlet energy transfer to $ZnPcIm_4$ with $\tau = 1.3$ ps. The redox potentials of both $ZnPcIm_4$ and PDI are similar so that electron transfer does not occur with this system. The lifetime of the lowest excited singlet state of $^1*(ZnPcIm_4)_7$ within $(\mathbf{16})_7$ displays a fast component ($\tau = 1.1$ ps) that depends quadratically on laser power due to singlet−singlet annihilation. This lifetime along with the known aggregate size and structure obtained from SAXS was used to determine that the singlet exciton hops between $ZnPcIm_4$ molecules in $\tau_{hop} = 160$ fs. Our results suggest that large artificial light harvesting systems having very rapid rates of energy migration can be obtained by self-assembly using this building block approach.

Self-Assembly Leading to Charge Separation. Strongly interacting π-stacked arrangements of chromophores are found in many biologically important molecules such as the primary electron donor within photosynthetic RC proteins and the base pairs within duplex DNA. In the former case, it has been proposed that symmetry breaking within the photoexcited singlet state of the special pair dimer results in significant intradimer charge-transfer character.[116−119] Photoexcitation of arene dimers constrained to a cofacial orientation usually leads to excimer formation,[120] while dimers bound in an edge-to-edge geometry with their π systems perpendicular to one another in the ground

state exhibit solvent-induced excited-state symmetry breaking in polar media.[121,122]

In an effort to develop more robust biomimetic electron donor−acceptor systems we have synthesized 1,7-bis(pyrrolidin-1′-yl)perylene-3,4:9,10-bis(dicarboximide) (5PDI),[123] a green chromophore with an intense absorption at 686 nm, having both electronics and redox properties that are remarkably similar to those of chlorophyll *a*.[98] Ultrafast transient absorption spectroscopy following excitation of the dimer with 700 nm, 100 fs laser pulses shows that quantitative intradimer electron transfer occurs within **17** in toluene with $\tau = 0.17$ ps followed by charge recombination to ground state with $\tau = 220$ ps. The symmetry breaking mechanism is most likely due to rotation of a pyrrolidine ring about the C−N bond joining it to the PDI core following photoexcitation,[124] leading to greater CT character in the excited state, and making the photoexcited 5PDI molecule a better electron donor, while the adjacent 5PDI molecule serves as the acceptor.

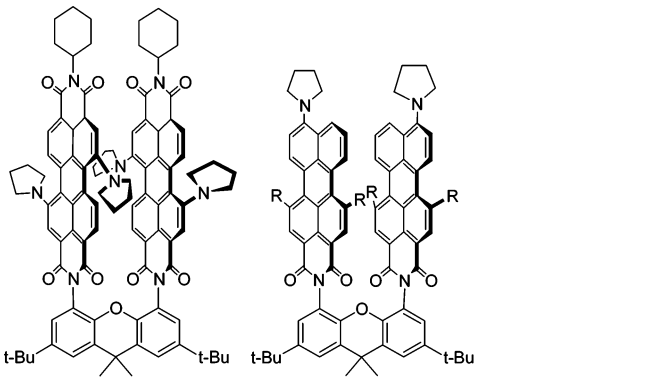

17 **18** (R = 3,5-di-tert-butylphenoxy)

We have examined the generality of symmetry-breaking leading to charge separation in arylene imides and diimides by preparing a symmetric cofacial dimer of 9-(*N*-pyrrolidinyl)-1,6-bis(3,5-di-*tert*-butylphenoxy)perylene-3,4-dicarboximide (5PMI), **18**. In this molecule, the pyrrolidine is attached to a different site of the arylene imide core relative to 5PDI resulting in another type of push−pull chromophore.[125] The CT transition in the ground-state absorption spectra of **18** is blue shifted, which is consistent with exciton coupling of the two face-to-face 5PMI chromophores. Ultrafast transient absorption spectroscopy following excitation of **18** with 400 nm, 80 fs laser pulses shows that quantitative intradimer electron transfer occurs in toluene with $\tau = 0.9$ ps followed by charge recombination to ground state with $\tau = 780$ ps. Excited-state symmetry breaking in the 5PDI and 5PMI dimers provides new routes to molecular assemblies for biomimetic charge separation and storage.

Given our observation that placing two "chlorophyll-like" 5PDI chromophores in a face-to-face configuration, **17**, leads to quantitative photoinduced charge separation, we reasoned that this same chromophore would be an excellent candidate for eliciting photochemical charge separation in a self-assembled, supramolecular system. The 5PDI chromophore does not have an intrinsic strong tendency to form aggregates, however, in contrast to PDI and its derivatives. This is due to steric hindrance to stacking imposed by the pyrrolidine rings at the 1 and 7 positions. We initially decided to apply well-known strategies used to produce discotic liquid crystals to induce assembly, where long alkyl chains are appended to aromatic core molecules to promote stacking through nanosegregation. Thus, we appended tris(*n*-dodecyloxy)phenyl groups to both imide nitrogens of 5PDI to give **19**, a molecule that self-assembles into ordered aggregates in nonpolar solvents and displays an LC phase.

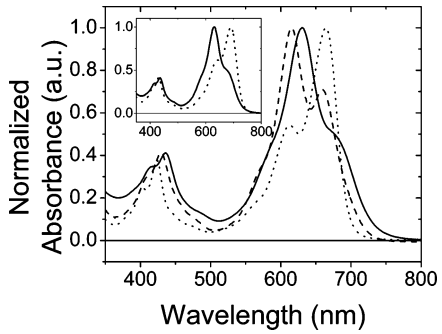

FIGURE 15. Electronic absorption spectra of **19** (−), **17** (- - -), and 5PDI (•••) in MCH. Inset: electronic absorption spectrum of **19** in toluene (- - -) and MCH (−).

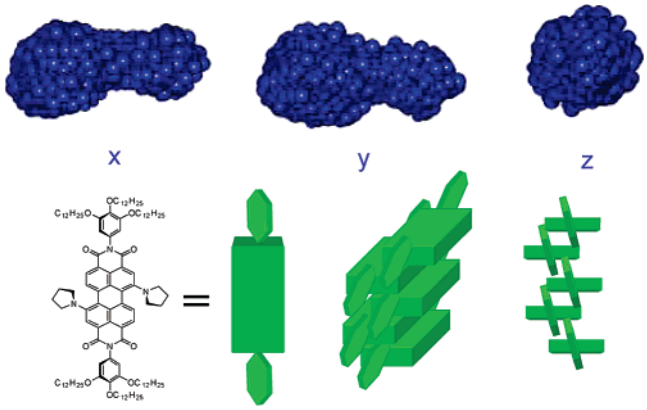

19

FIGURE 16. Aggregate structure of **19** in solution (10^{-4} M) with dimensions 3.6 × 2.0 × 1.8 nm. Model of the arrangement of $(\mathbf{19})_5$ based on the steric demand of the 3,4,5-trialkoxyphenyl groups, which are 78° out-of-plane with the 5PDI core chromophore.

The ground-state absorption spectrum of 10^{-4}M **19** in MCH is given in Figure 15 and shows features indicative of H-aggregate formation. That spectrum is compared with those of covalent 5PDI dimer **17** and a monomeric 5PDI reference compound bearing *N*-cyclohexyl substituents that does not aggregate in MCH. Molecule **19** displays an absorption maximum at 630 nm in MCH with a weaker shoulder near 670 nm. For comparison, the absorption spectrum of 5PDI in MCH has maximum absorbance at 665 nm and is very similar to that in toluene. In MCH, the optical absorption spectrum of **17** shows a peak at 615 nm and a shoulder at 660 nm, and very closely resembles that of **19**. To estimate the aggregate size and shape of **19** in MCH solution, we performed SAXS measurements as noted above. Analysis of the data using pair distribution function and simulating annealing procedures shows that **19** self-assembles into monodisperse pentamers at 10^{-4} M, Figure 16.[126]

Transient absorption measurements carried out on **19** in MCH and toluene, Figure 17, show that in MCH the bleach of the ground-state absorption band at 630 nm is accompanied by the formation of a 760 nm absorption band, both of which appear within the 0.13 ps instrument response function (IRF) of the experiment. In toluene the ground-state bleach at 700 nm also occurs within the IRF, but the band at 760 nm does not appear. The absorption changes of **19** at both 630 and 760 nm in MCH

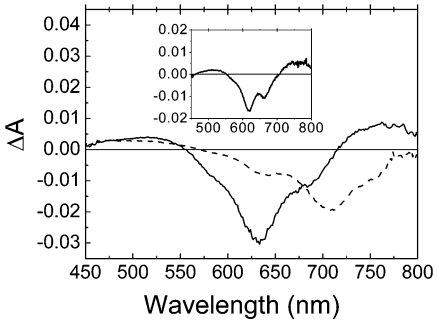

FIGURE 17. Transient absorption spectra of **19** in MCH (−) and toluene (- - -) 269 ps after excitation with a 400 nm, 80 fs laser pulse. Inset: transient absorption spectrum of **17** in MCH (−) 156 ps after excitation with a 400 nm, 80 fs laser pulse.

both decay with $\tau = 860$ ps, while the 700 nm bleach of **19** in toluene decays with $\tau = 4.5$ ns, the lifetime of the lowest excited singlet state of the 5PDI monomer.[127] The transient absorption spectrum of **17** obtained in MCH is shown in the inset to Figure 17. This spectrum is very similar to that of $(\mathbf{19})_5$ in MCH solution, as evidenced by the absorbance bleach at 630 nm and the positive ΔA feature at 710−800 nm. These transient spectral features both decay with $\tau = 1050$ ps. Our earlier work on **17** showed that the transient absorption feature at 710−800 nm is due to the formation of $5PDI^{-\bullet}$ that results from excited-state symmetry breaking leading to $5PDI^{+\bullet}-5PDI^{-\bullet}$.[127] The formation of the 760 nm absorption band for both **17** and $(\mathbf{19})_5$ in MCH shows that this same process leads to the formation of $5PDI^{+\bullet}-5PDI^{-\bullet}$.

Combining Reaction Center and Antenna Function. Several fully covalent systems have been constructed where the light harvesting, energy funneling, and charge separation functions of the photosynthetic reaction center are successfully mimicked. For example, within the zinc porphyrin (ZnP)-free base porphyrin (HP)-C_{60} molecular triad, **20**, excitation of the zinc porphyrin antenna leads to singlet−singlet energy transfer to the free base porphyrin, which then donates an electron to the fullerene in 25 ps. A subsequent hole transfer produces the $ZnP^{+}-HP-C_{60}^{-}$ final charge-separated state in quantum yields >90% following excitation of any of the three chromophores.[128]

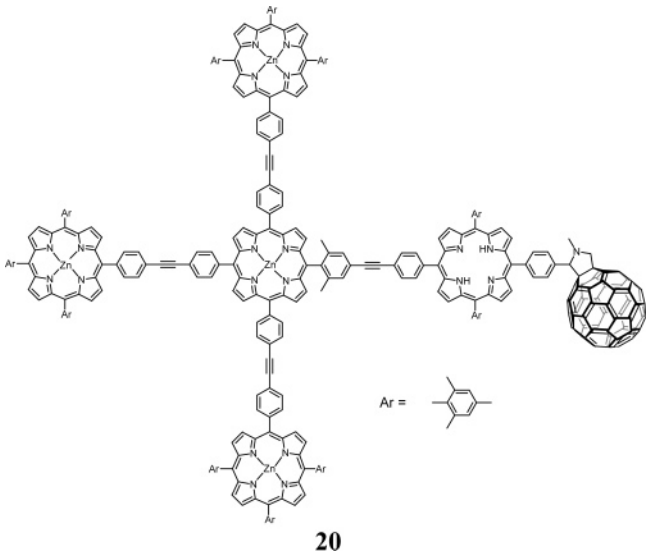

20

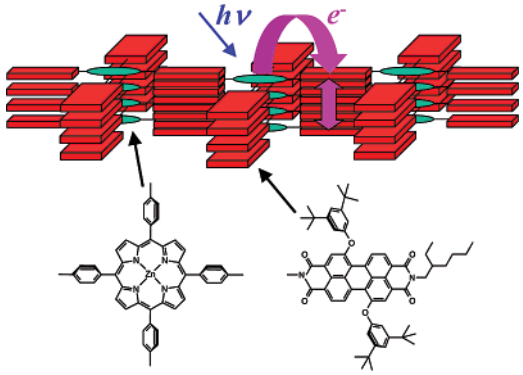

FIGURE 18. Proposed structure of self-assembled $(ZnTPP-PDI_4)_n$.

Molecules that contain multiple imide linkages can be used to develop artificial systems that mimic light harvesting and photoinduced charge separation within photosynthetic proteins as well. Quite often, these molecules contain redox active chromophores that utilize $\pi-\pi$ interactions to self-assemble into supramolecular arrays.[93,123,129−138] The robust nature of the arylene imide and bis(imide) chromophores makes them appealing candidates for the development of integrated light harvesting and charge separation systems for artificial photosynthesis.

For example, we have demonstrated that a molecule having four PDI electron-accepting chromophores attached to a central zinc 5,10,15,20-tetraphenylporphyrin (ZnTPP) electron donor self-assembles into ordered arrays both in solution and in the solid-state driven by $\pi-\pi$ interactions of the PDI molecules.[111] The optical spectra of $(ZnTPP-PDI_4)_n$ strongly support the proposed structure depicted schematically in Figure 18. The PDI molecules stack directly on top of one another, at a van der Waals contact distance of about 3.5 Å, while the ZnTPP molecules occupy sites in every other layer with an interlayer Zn−Zn distance of about 7Å. Photoexcitation of the arrays results in quantitative charge separation in 3.2 ps to form $ZnTPP^{+\bullet}$ $PDI^{-\bullet}$ radical ion pairs in which the radical anion rapidly migrates to PDI molecules as much as 4 nm away as evidenced by the MFE on the yield of the PDI triplet state that results from radical ion pair recombination.

Based on our experience with using self-assembly to induce a face-to-face geometry that promotes charge separation within **19**, we decided to use the well-known aggregation properties of PDI chromophores to carry out the function of bringing two 5PDI molecules close to one another as well as providing a light-harvesting antenna array. We have reported the synthesis and characterization of **21**, which self-assembles into stacked dimers $(\mathbf{21})_2$ in solution as revealed by SAXS, Figure 19.[139] This dimeric array demonstrates that self-assembly of a robust PDI-based artificial light-harvesting antenna structure induces self-assembly of a functional special pair of 5PDI molecules that undergoes ultrafast, quantitative charge separation. The structure consists of four PDI molecules attached to a single 5PDI core, which self-assembles to form $(\mathbf{21})_2$ in toluene. Femtosecond transient absorption spectroscopy, Figure 20, shows that energy transfer from $(PDI)_2$ to $(5PDI)_2$ occurs with $\tau = 21$ ps, followed by excited-state symmetry breaking of $^1*(5PDI)_2$ to produce $5PDI^{+\bullet}-5PDI^{-\bullet}$ quantitatively with $\tau_{CS} = 7$ ps. The ion pair recombines with $\tau_{CR} = 420$ ps. Electron transfer occurs only in the dimeric system, and does not occur in the disassembled monomer, thus mimicking both antenna and

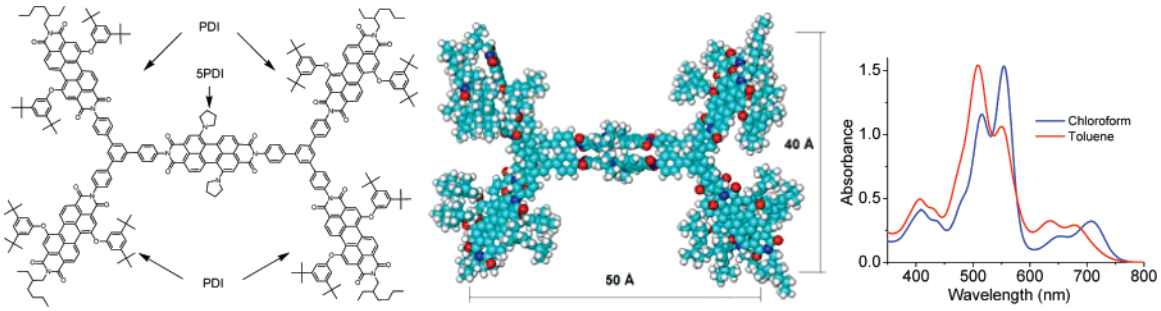

FIGURE 19. Chemical structure of **21** (left), the best fit structure of $(\mathbf{21})_2$ from modeling the SAXS data (center), and the UV−vis spectra showing dimerization in toluene (monomers in $CHCl_3$) and excellent solar spectral coverage (right).

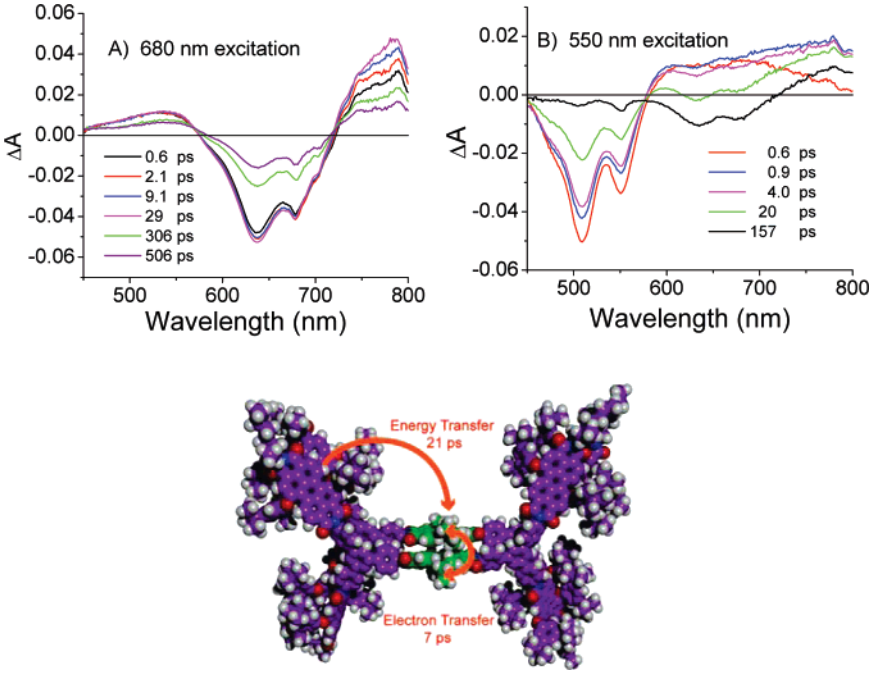

FIGURE 20. Transient absorption spectra of $(\mathbf{21})_2$ in toluene following laser excitation at (A) 680 nm and (B) 550 nm.

special pair function in photosynthesis. The charge separation observed in $(\mathbf{21})_2$ is an example of emergent behavior that is not present when monomeric **21** is photoexcited.

Future Prospects

The field of artificial photosynthesis has developed in parallel with those of supramolecular chemistry and nanoscale materials chemistry. In addition, it has taken advantage of advances in synthetic methodology, time-resolved spectroscopy, and structural characterization. From a different perspective, the worldwide effort over the past three decades to understand the molecular mechanisms of charge separation and storage in natural photosynthesis and the accompanying efforts to achieve artificial photosynthesis have provided the impetus to develop the related science and technology necessary to accomplish these goals. There are numerous important and challenging problems remaining in this field, and it is my view that the most difficult challenges remain ahead of us. Some of these challenges are detailed in the next few paragraphs.

A deeper fundamental understanding of how the molecular dynamics of the bridge molecules in a donor−bridge−acceptor (D−B−A) system control long distance electron transport from D to A needs to be obtained by attacking this problem on multiple time and length scales. For example, at short times new techniques in time-resolved Raman spectroscopy that preserve spectral resolution,[140,141] while permitting subpicosecond time resolution can be used to study how specific molecular motions are coupled to photoinduced charge separation. In addition, modern methods in time-resolved EPR spectroscopy can be used to probe the dynamics of charge recombination on a nanosecond time scale, while providing significant structural detail.[84]

The fundamental requirements for photoinduced charge transport in self-assembled systems are as yet poorly understood. The preparation and characterization of new covalent building blocks that both initiate photoinduced charge separation, and promote long distance charge transport by self-assembling into extended noncovalent structures is needed to build functional systems. In addition, the development of antenna-reaction center systems in which self-assembly of the antenna elicits formation of a reaction center capable of separating charge for times sufficiently long to promote long distance charge transport is an important next step to integrate multiple tasks for artificial photosynthesis. Achieving these goals will require a knowledge

of how self-assembly using π-stacking can be combined with hydrogen bonding to simplify the structure of the building blocks, and yet retain the overall ability to assemble a complex, photofunctional structure. Important new tools that are being developed to relate supramolecular structure to function include time-resolved X-ray scattering techniques using synchrotron sources.[142,143]

Most catalysts for fuel forming reactions, such as water splitting and CO_2 reduction, require charge accumulation at a central redox site, while current artificial photosynthetic systems provide one radical ion pair for every photon absorbed. New insights into how multiple photoinduced charge separation pathways can be used to accumulate several redox equivalents at a single redox site are needed to meet the requirements of multielectron catalysts. In addition, new catalysts that can use the accumulated redox equivalents generated by a sequence of single electron-transfer events to drive water oxidation and carbon dioxide reduction are required.

As our understanding of self-assembly increases to the point where functional, integrated artificial photosynthetic systems are built, it will be important to take advantage of bio-inspired self-repair strategies to ensure that the functional assembly can survive the damage that is inevitable when thermodynamically demanding reactions are carried out. At this point, very little is known on how to address this problem, yet solving it provides an important and exciting scientific challenge.

Acknowledgment. First and foremost, I thank the graduate students and postdocs who have been my tireless co-workers. Their names are given in the references. I would also like to thank Profs. Haim Levanon (Hebrew University of Jerusalem), Mark Ratner (Northwestern), and Frederick Lewis (Northwestern), who have been my long-time collaborators on electron-transfer problems. I am also grateful to Dr. David Tiede (Argonne National Laboratory) for introducing us to using SAXS to determine supramolecular structures in solution and for subsequent collaborative work. I also wish to acknowledge support from the Division of Chemical Sciences, Office of Basic Energy Sciences, U.S. Department of Energy under Grant No. DE-FG02-99ER14999.

References

(1) Blankenship, R. E. *Molecular Mechanisms of Photosynthesis*; Blackwell Science: Oxford, 2002.
(2) Ferreira, K. N.; Iverson, T. M.; Maghlaoui, K.; Barber, J.; Iwata, S. *Science* **2004**, *303*, 1831−1838.
(3) Deisenhofer, J.; Epp, O.; Miki, K.; Huber, R.; Michel, H. *J. Mol. Biol.* **1984**, *180*, 385−398.
(4) Allen, J. P.; Feher, G.; Yeates, T. O.; Komiya, H.; Rees, D. C. *Proc. Natl. Acad. Sci. U.S.A.* **1987**, *84*, 5730−5734.
(5) Chang, C. H.; El-Kabbani, O.; Tiede, D.; Norris, J.; Schiffer, M. *Biochemistry* **1991**, *30*, 5352−5360.
(6) Woodbury, N. W.; Allen, J. P. In *Anoxygenic Photosynthetic Bacteria*; Blankenship, R. E., Madigan, M. T., Bauer, C. E., Eds.; Kluwer Academic Publishers: Dordrecht, 1995; pp 527−557.
(7) Dutton, P. L.; Leigh, J. S.; Seibert, M. *Biochem. Biophys. Res. Commun.* **1972**, *46*, 406−413.
(8) Thurnauer, M. C.; Katz, J. J.; Norris, J. R. *Proc. Natl. Acad. Sci. U.S.A.* **1975**, *72*, 3270−3274.
(9) Marcus, R. A. *J. Chem. Phys.* **1956**, *24*, 966−978.
(10) Hush, N. S. *J. Chem. Phys.* **1958**, *28*, 962−972.
(11) Levich, V. G.; Dogonadze, R. R. *Collect. Czech. Chem. Commun.* **1961**, *26*, 193-214.
(12) Jortner, J. *J. Chem. Phys.* **1976**, *64*, 4860−4867.
(13) Miller, J. R.; Calcaterra, L. T.; Closs, G. L. *J. Am. Chem. Soc.* **1984**, *106*, 3047−3049.
(14) Wasielewski, M. R.; Niemczyk, M. P.; Svec, W. A.; Pewitt, E. B. *J. Am. Chem. Soc.* **1985**, *107*, 1080−1082.
(15) Paddon-Row: M. N.; Oliver, A. M.; Warman, J. M.; Smit, K. J.; de Haas, M. P.; Oevering, H.; Verhoeven, J. W. *J. Phys. Chem.* **1988**, *92*, 6958−6962.
(16) Moser, C. C.; Keske, J. M.; Warncke, K.; Farid, R. S.; Dutton, P. L. *Nature (London)* **1992**, *355*, 796−802.
(17) Winkler, J. R.; Gray, H. B. *Chem. Rev.* **1992**, *92*, 369−379.
(18) Holmlin, R. E.; Dandliker, P. J.; Barton, J. K. *Angew. Chem., Int. Ed.* **1998**, *36*, 2714-2730.
(19) Lewis, F. D.; Wu, T.; Zhang, Y.; Letsinger, R. L.; Greenfield, S. R.; Wasielewski, M. R. *Science (Washington, D. C.)* **1997**, *277*, 673−676.
(20) Johnson, M. D.; Miller, J. R.; Green, N. S.; Closs, G. L. *J. Phys. Chem.* **1989**, *93*, 1173−1176.
(21) Oevering, H.; Paddon-Row: M. N.; Heppener, M.; Oliver, A. M.; Cotsaris, E.; Verhoeven, J. W.; Hush, N. S. *J. Am. Chem. Soc.* **1987**, *109*, 3258−3269.
(22) Helms, A.; Heiler, D.; McLendon, G. *J. Am. Chem. Soc.* **1992**, *114*, 6227−6238.
(23) Ribou, A.-C.; Launay, J.-P.; Takahashi, K.; Nihira, T.; Tarutani, S.; Spangler, C. W. *Inorg. Chem.* **1994**, *33*, 1325−1329.
(24) De Cola, L.; Belser, P. *Coord. Chem. Rev.* **1998**, *177*, 301−346.
(25) Weiss, E. A.; Ahrens, M. J.; Sinks, L. E.; Gusev, A. V.; Ratner, M. A.; Wasielewski, M. R. *J. Am. Chem. Soc.* **2004**, *126*, 5577−5584.
(26) Arrhenius, T. S.; Blanchard-Desce, M.; Dvolaitzky, M.; Lehn, J. M.; Malthete, J. *Proc. Natl. Acad. Sci. U.S.A.* **1986**, *83*, 5355−5359.
(27) Effenberger, F.; Wolf, H. C. *New J. Chem.* **1991**, *15*, 117−123.
(28) Tolbert, L. M. *Acc. Chem. Res.* **1992**, *25*, 561−568.
(29) Wasielewski, M. R.; Johnson, D. G.; Svec, W. A.; Kersey, K. M.; Cragg, D. E.; Minsek, D. W. In *Photochemical Energy Conversion, Proceedings of the International Conference on Photochemical Conversion and Storage of Solar Energy, 7th*; Norris, J. R., Ed.; Elsevier: New York, 1989; pp 135−147.
(30) Grosshenny, V.; Harriman, A.; Ziessel, R. *Angew. Chem., Int. Ed. Engl.* **1996**, *34*, 2705−2708.
(31) Sachs, S. B.; Dudek, S. P.; Hsung, R. P.; Sita, L. R.; Smalley, J. F.; Newton, M. D.; Feldberg, S. W.; Chidsey, C. E. D. *J. Am. Chem. Soc.* **1997**, *119*, 10563−10564.
(32) Tour, J. M. *Chem. Rev.* **1996**, *96*, 537−553.
(33) McConnell, H. M. *J. Chem. Phys.* **1961**, *35*, 508−515.
(34) Won, Y.; Friesner, R. A. *Biochim. Biophys. Acta* **1988**, *935*, 9−18.
(35) Closs, G. L.; Miller, J. R. *Science* **1988**, *240*, 440−447.
(36) Roest, M. R.; Oliver, A. M.; Paddon-Row: M. N.; Verhoeven, J. W. *J. Phys. Chem. A* **1997**, *101*, 4867.
(37) Davis, W. B.; Wasielewski, M. R.; Ratner, M. A.; Mujica, V.; Nitzan, A. *J. Phys. Chem.* **1997**, *101*, 6158−6164.
(38) Davis, W. B.; Svec, W. A.; Ratner, M. A.; Wasielewski, M. R. *Nature* **1998**, *396*, 60−63.
(39) Maruyama, K.; Osuka, A. *Pure Appl. Chem.* **1990**, *62*, 1511−1520.
(40) Wasielewski, M. R. *Chem. Rev.* **1992**, *92*, 435−461.
(41) Gust, D.; Moore, T. A.; Moore, A. L. *Acc. Chem. Res.* **1993**, *26*, 198−205.
(42) Gust, D.; Moore, T. A. In *The Porphyrin Handbook*; Kadish, K. M., Smith, K. M., Guilard, R., Eds.; Academic Press: San Diego, 2000; Vol. 8, pp 153−190.
(43) Guldi, D. M.; Imahori, H. *J. Porphyrins Phthalocyanines* **2004**, *8*, 976−983.
(44) Imahori, H. *J. Phys. Chem. B* **2004**, *108*, 6130−6143.
(45) Gaines, G. L., III; O'Neil, M. P.; Svec, W. A.; Niemczyk, M. P.; Wasielewski, M. R. *J. Am. Chem. Soc.* **1991**, *113*, 719−721.
(46) Moore, T. A.; Gust, D.; Mathis, P.; Mialocq, J. C.; Chachaty, C.; Bensasson, R. V.; Land, E. J.; Doizi, D.; Liddell, P. A.; et al. *Nature (London, U.K.)* **1984**, *307*, 630−632.
(47) Kuciauskas, D.; Liddell, P. A.; Lin, S.; Stone, S. G.; Moore, A. L.; Moore, T. A.; Gust, D. *J. Phys. Chem. B* **2000**, *104*, 4307−4321.
(48) Gust, D.; Moore, T. A.; Moore, A. L.; Lee, S. J.; Bittersmann, E.; Luttrull, D. K.; Rehms, A. A.; DeGraziano, J. M.; Ma, X. C.; et al. *Science (Washington, DC)* **1990**, *248*, 199−201.
(49) Wasielewski, M. R.; Gaines, G. L., III; O'Neil, M. P.; Svec, W. A.; Niemczyk, M. P. *J. Am. Chem. Soc.* **1990**, *112*, 4559−4560.
(50) Lepley, A. R., Closs, G. L., Eds. *Chem. Induced Magn. Polariz.* **1973**.
(51) Wasielewski, M. R.; Gaines, G. L., III; Wiederrecht, G. P.; Svec, W. A.; Niemczyk, M. P. *J. Am. Chem. Soc.* **1993**, *115*, 10442−10443.
(52) Marcus, R. A. *Chem. Phys. Lett.* **1987**, *133*, 471.
(53) Ogrodnik, A.; Michel-Beyerle, M. E. *Z. Naturforsch.* **1989**, *44a*, 763−764.
(54) Kilsa, K.; Kajanus, J.; Macpherson, A. N.; Martensson, J.; Albinsson, B. *J. Am. Chem. Soc.* **2001**, *123*, 3069−3080.
(55) Lukas, A. S.; Bushard, P. J.; Wasielewski, M. R. *J. Phys. Chem. A* **2002**, *106*, 2074−2082.
(56) Kramers, H. A. *Physica* **1934**, *1*, 182−192.
(57) Anderson, P. W. *Phys. Rev.* **1950**, *79*, 350−356.
(58) Anderson, P. W. *Phys. Rev.* **1959**, *115*, 2−13.
(59) Marcus, R. A. *J. Chem. Phys.* **1965**, *43*, 679−701.
(60) Yamashita, J.; Kondo, J. *Phys. Rev.* **1958**, *109*, 730−741.
(61) Closs, G. L.; Piotrowiak, P. J.; MacInnis, J. M.; Fleming, G. R. *J. Am. Chem. Soc.* **1988**, *110*, 2652−2653.
(62) Feher, G.; Okamura, M. In *Tunneling Conference*; Chance, B., Devault, D., Frauenfelder, H., Marcus, R. A., Schreiffer, J. R., Sutin, N., Eds.; Academic Press: New York, 1979; pp 729−743.

(63) Weiss, E. A.; Sinks, L. E.; Lukas, A. S.; Chernick, E. T.; Ratner, M. A.; Wasielewski, M. R. *J. Phys. Chem. B* **2004**, *108*, 10309−10316.
(64) Kobori, Y.; Sekiguchi, S.; Akiyama, K.; Tero-Kubota, S. *J. Phys. Chem. A* **1999**, *103*, 5416−5424.
(65) Paddon-Row: M. N.; Shephard, M. J. *J. Phys. Chem. A* **2002**, *106*, 2935−2944.
(66) Volk, M.; Haberle, T.; Feick, R.; Ogrodnik, A.; Michel-Beyerle, M. E. *J. Phys. Chem.* **1993**, *97*, 9831−9836.
(67) Weller, A.; Staerk, H.; Treichel, R. *Faraday Discuss., Chem. Soc.* **1984**, *78*, 271−278.
(68) Hoff, A. J.; Gast, P.; van der Vos, R.; Franken, E. M.; Lous, E. J. *Z. Phys. Chem.* **1993**, *180*, 175−192.
(69) Till, U.; Hore, P. J. *Mol. Phys.* **1997**, *90*, 289−296.
(70) Steiner, U. E.; Ulrich, T. *Chem. Rev.* **1989**, *89*, 51−147.
(71) Schulten, K.; Staerk, H.; Weller, A.; Werner, H.-J.; Nickel, B. *Z. Phys. Chem.* **1976**, *101*, 371−390.
(72) Tanimoto, Y.; Okada, N.; Itoh, M.; Iwai, K.; Sugioka, K.; Takemura, F.; Nakagaki, R.; Nagakura, S. *Chem. Phys. Lett.* **1987**, *136*, 42−46.
(73) Sakaguchi, Y.; Hayashi, H. *J. Phys. Chem. A* **1997**, *101*, 549−555.
(74) Werner, U.; Kuhnle, W.; Staerk, H. *J. Phys. Chem.* **1993**, *97*, 9280−9287.
(75) Weiss, E. A.; Ratner, M. A.; Wasielewski, M. R. *J. Phys. Chem. A* **2003**, *107*, 3639−3647.
(76) Lukas, A. S.; Bushard, P. J.; Weiss, E. A.; Wasielewski, M. R. *J. Am. Chem. Soc.* **2003**, *125*, 3921−3930.
(77) Tadjikov, B.; Smirnov, S. *Phys. Chem. Chem. Phys.* **2001**, *3*, 204−212.
(78) Tsentalovich, Y. P.; Morozova, O. B.; Avdievich, N. I.; Ananchenko, G. S.; Yurkovskaya, A. V.; Ball, J. D.; Forbes, M. D. E. *J. Phys. Chem. A* **1997**, *101*, 8809−8816.
(79) Blankenship, R. E.; Schaafsma, T. J.; Parson, W. W. *Biochim. Biophys. Acta* **1977**, *461*, 297−305.
(80) Plato, M.; Möbius, K.; Michel-Beyerle, M. E.; Bixon, M.; Jortner, J. *J. Am. Chem. Soc.* **1988**, *110*, 7279−7285.
(81) Werner, H.-J.; Schulten, K.; Weller, A. *Biochim. Biophys. Acta* **1978**, *502*, 255−268.
(82) Norris, J. R.; Bowman, M. K.; Budil, D. E.; Tang, J.; Wraight, C. A.; Closs, G. L. *Proc. Natl. Acad. Sci. U.S.A.* **1982**, *79*, 5532−5536.
(83) Shultz, D. A.; Fico, R. M., Jr.; Bodnar, S. H.; Kumar, R. K.; Vostrikova, K. E.; Kampf, J. W.; Boyle, P. D. *J. Am. Chem. Soc.* **2003**, *125*, 11761−11771.
(84) Schweiger, A.; Jeschke, G. *Principles of pulsed electron paramagnetic resonance*; Oxford: Oxford, 2001.
(85) Hasharoni, K.; Levanon, H.; Greenfield, S. R.; Gosztola, D. J.; Svec, W. A.; Wasielewski, M. R. *J. Am. Chem. Soc.* **1995**, *117*, 8055−8056.
(86) Hasharoni, K.; Levanon, H.; Greenfield, S. R.; Gosztola, D. J.; Svec, W. A.; Wasielewski, M. R. *J. Am. Chem. Soc.* **1996**, *118*, 10228−10235.
(87) Carbonera, D.; DiValentin, M.; Corvaja, C.; Agostini, G.; Giacometti, G.; Liddell, P. A.; Kuciauskas, D.; Moore, A. L.; Moore, T. A.; Gust, D. *J. Am. Chem. Soc.* **1998**, *120*, 4398−4405.
(88) Shaakov, S.; Galili, T.; Stavitski, E.; Levanon, H.; Lukas, A.; Wasielewski, M. R. *J. Am. Chem. Soc.* **2003**, *125*, 6563−6572.
(89) Hore, P. J.; Hunter, D. A.; McKie, C. D.; Hoff, A. J. *Chem. Phys. Lett.* **1987**, *137*, 495−500.
(90) Norris, J. R.; Morris, A. L.; Thurnauer, M. C.; Tang, J. *J. Chem. Phys.* **1990**, *92*, 4239−4249.
(91) Levanon, H.; Hasharoni, K. *Prog. Reac. Kinet.* **1995**, *20*, 309−346.
(92) Levanon, H.; Norris, J. R. *Chem. Rev.* **1978**, *78*, 185−198.
(93) Greenfield, S. R.; Svec, W. A.; Gosztola, D.; Wasielewski, M. R. *J. Am. Chem. Soc.* **1996**, *118*, 6767−6777.
(94) Hasharoni, K.; Levanon, H. *J. Phys. Chem.* **1995**, *99*, 4875−4878.
(95) Andersson, M.; Sinks, L. E.; Hayes, R. T.; Zhao, Y.; Wasielewski, M. R. *Angew. Chem., Int. Ed.* **2003**, *42*, 3139−3143.
(96) Mori, Y.; Sakaguchi, Y.; Hayashi, H. *Chem. Phys. Lett.* **1998**, *286*, 446−451.
(97) Mori, Y.; Sakaguchi, Y.; Hayashi, H. *J. Phys. Chem. A* **2002**, *106*, 4453−4467.
(98) Lukas, A. S.; Bushard, P.; Wasielewski, M. R. *J. Phys. Chem. A* **2002**, *106*, 2074−2082.
(99) Weiss, E. A.; Tauber, M. J.; Kelley, R. F.; Ahrens, M. J.; Ratner, M. A.; Wasielewski, M. R. *J. Am. Chem. Soc.* **2005**, *127*, 11842−11850.
(100) Cacelli, I.; Prampolini, G. *J. Phys. Chem. A* **2003**, *107*, 8665−8670.
(101) Melzer, P.; Kurreck, H.; Kieslich, W. *Chem. Ber.* **1982**, *115*, 3597−3609.
(102) Goldsmith, R. H.; Sinks, L. E.; Kelley, R. F.; Betzen, L. J.; Liu, W. H.; Weiss, E. A.; Ratner, M. A.; Wasielewski, M. R. *Proc. Natl. Acad. Sci. U.S.A.* **2005**, *102*, 3540−3545.
(103) Sundstrom, V.; Pullerits, T.; van Grondelle, R. *J. Phys. Chem. B* **1999**, *103*, 2327−2346.
(104) Seth, J.; Palaniappan, V.; Wagner, R. W.; Johnson, T. E.; Lindsey, J. S.; Bocian, D. F. *J. Am. Chem. Soc.* **1996**, *118*, 11194−11207.
(105) Aratani, N.; Osuka, A. *Bull. Chem. Soc. Jpn.* **2001**, *74*, 1361−1379.
(106) Kim, D.; Osuka, A. *Acc. Chem. Res.* **2004**, *37*, 735−745.
(107) Worcester, D. L.; Michalski, T. J.; Katz, J. J. *Proc. Natl. Acad. Sci. U.S.A.* **1986**, *83*, 3791−3795.
(108) Tamiaki, H. *Coord. Chem. Rev.* **1996**, *148*, 183−197.
(109) Ahrens, M. J.; Sinks, L. E.; Rybtchinski, B.; Liu, W.; Jones, B. A.; Giaimo, J. M.; Gusev, A. V.; Goshe, A. J.; Tiede, D. M.; Wasielewski, M. R. *J. Am. Chem. Soc.* **2004**, *126*, 8284−8294.
(110) Kasha, M.; Rawles, H. R.; El-Bayoumi, M. L. *Pure Appl. Chem* **1965**, *11*, 371−392.
(111) van der Boom, T.; Hayes, R. T.; Zhao, Y.; Bushard, P. J.; Weiss, E. A.; Wasielewski, M. R. *J. Am. Chem. Soc.* **2002**, *124*, 9582−9590.
(112) Li, X.; He, X.; Ng, A. C. H.; Ng, D. K. P.; Wu, C. *Macromolecules* **2000**, *33*, 2119−2123.
(113) Tiede, D. M.; Zhang, R.; Chen, L. X.; Yu, L.; Lindsey, J. S. *J. Am. Chem. Soc.* **2004**, *126*, 14054−14062.
(114) Guinier, A.; Fournet, G. *Small Angle Scattering of X-rays*; Wiley: New York, 1955.
(115) Svergun, D. I.; Koch, M. H. *Rep. Prog. Phys.* **2003**, *66*, 1735−1782.
(116) Lathrop, E. J. P.; Friesner, R. A. *J. Phys. Chem.* **1994**, *98*, 3056−3066.
(117) Won, Y.; Friesner, R. A. *Proc. Natl. Acad. Sci. U.S.A.* **1987**, *84*, 5511−5515.
(118) Parson, W. W.; Scherz, A.; Warshel, A. *Springer Ser. Chem. Phys.* **1985**, *42*, 112−130.
(119) Laporte, L. L.; Palaniappan, V.; Kirmaier, C.; Davis, D. G.; Schenck, C. C.; Holten, D.; Bocian, D. F. *J. Phys. Chem.* **1996**, *100*, 17696−17707.
(120) Staab, H. A.; Riegler, N.; Diederich, F.; Krieger, C.; Schweitzer, D. *Chem. Ber.* **1984**, *117*, 246−259.
(121) Rettig, W. *Angew. Chem., Int. Ed. Engl.* **1986**, *25*, 971−988.
(122) Kang, T. J.; Kahlow, M. A.; Giser, D.; Swallen, S.; Nagarajan, N.; Jarzeba, W.; Barbara, P. F. *J. Phys. Chem.* **1988**, *92*, 6800−6807.
(123) Zhao, Y.; Wasielewski, M. R. *Tetrahedron Lett.* **1999**, *40*, 7047−7050.
(124) Lukas, A. S.; Zhao, Y.; Miller, S. E.; Wasielewski, M. R. *J. Phys. Chem. B* **2002**, *106*, 1299−1306.
(125) Miller, S. E.; Schaller, R.; Mulloni, V.; Zhao, Y.; Just, E. M.; Johnson, R. C.; Wasielewski, M. R. *Chem. Phys.* **2002**, *275*, 167−183.
(126) Volkov, V. V.; Svergun, D. I. *J. Appl. Crystallogr.* **2003**, *36*, 860−864.
(127) Giaimo, J. M.; Gusev, A. V.; Wasielewski, M. R. *J. Am. Chem. Soc.* **2002**, *124*, 8530−8531.
(128) Liddell, P. A.; Kodis, G.; Kuciauskas, D.; Andreasson, J.; Moore, A. L.; Moore, T. A.; Gust, D. *Phys. Chem. Chem. Phys.* **2004**, *6*, 5509−5515.
(129) Beckers, E. H. A.; Jonkheijm, P.; Schenning, A. P. H. J.; Meskers, S. C. J.; Janssen, R. A. J. *ChemPhysChem* **2005**, *6*, 2029−2031.
(130) Ahrens, M. J.; Sinks, L. E.; Rybtchinski, B.; Liu, W.; Jones, B. A.; Giaimo, J. M.; Gusev, A. V.; Goshe, A. J.; Tiede, D. M.; Wasielewski, M. R. *J. Am. Chem. Soc.* **2004**, *126*, 8284−8294.
(131) Herrikhuyzen, J. v.; Syamakumari, A.; Schenning, A. P. H. J.; Meijer, E. W. *J. Am. Chem. Soc.* **2004**, *126*, 10021−10027.
(132) Ramos, A. M.; Meskers, S. C. J.; Beckers, E. H. A.; Prince, R. B.; Brunsveld, L.; Janssen, R. A. J. *J. Am. Chem. Soc.* **2004**, *126*, 9630−9644.
(133) Würthner, F. *Chem. Commun.* **2004**, 1564−1579.
(134) Hayes, R. T.; Walsh, C. J.; Wasielewski, M. R. *J. Phys. Chem. A* **2004**, *108*, 3253−3260.
(135) Freiburg, H. G., Nitzan, A., Eds. *Special Issue: The Spin-Boson Problem: From Electron Transfer to Quantum Computing...to the 60th Birthday of Professor Ulrich Weiss. Chem. Phys.* **2004**, *296* (2−3).
(136) Schmidt-Mende, L.; Fechtenkotter, A.; Müllen, K.; Moons, E.; Friend, R. H.; MacKenzie, J. D. *Science* **2001**, *293*, 1119−1122.
(137) Ramos, A. M.; Rispens, M. T.; van Duren, J. K. J.; Hummelen, J. C.; Janssen, R. A. J. *J. Am. Chem. Soc.* **2001**, *123*, 6714−6715.
(138) Holtrup, F. O.; Muller, G. R. J.; Quante, H.; De Feyter, S.; De Schryver, F. C.; Müllen, K. *Chem. Eur. J.* **1997**, *3*, 219−225.
(139) Rybtchinski, B.; Sinks, L. E.; Wasielewski, M. R. *J. Am. Chem. Soc.* **2004**, *126*, 12268−12269.
(140) Kukura, P.; McCamant, D. W.; Yoon, S.; Wandschneider, D. B.; Mathies, R. A. *Science (Washington, DC)* **2005**, *310*, 1006−1009.
(141) McCamant, D. W.; Kukura, P.; Mathies, R. A. *J. Phys. Chem. B* **2005**, *109*, 10449−10457.
(142) Khodakov, A. Y.; Zholobenko, V. L.; Imperor-Clerc, M.; Durand, D. *J. Phys. Chem. B* **2005**, *109*, 22780−22790.
(143) Sakurai, K.; Jeong, Y.; Koumoto, K.; Friggeri, A.; Gronwald, O.; Sakurai, S.; Okamoto, S.; Inoue, K.; Shinkai, S. *Langmuir* **2003**, *19*, 8211−8217.

JO060225D